
Don't Use Large Mini-Batches, Use Local SGD

Tao Lin¹ Sebastian U. Stich¹ Kumar Kshitij Patel¹ Martin Jaggi¹

Abstract

Mini-batch stochastic gradient methods are state of the art for distributed training of deep neural networks. In recent years, a push for efficiency for large-scale applications has lead to drastically large mini-batch sizes. However, two significant roadblocks remain for such large-batch variants. On one hand, increasing the number of workers introduces communication bottlenecks, and efficient algorithms need to be able to adapt to the changing computation vs. communication trade-offs in heterogeneous systems. On the other hand, independent of communication, large-batch variants do not generalize well.

We argue that variants of recently proposed local SGD, which performs several update steps on a local model before communicating with other workers can solve both these problems. Our experiments show performance gains in training efficiency, scalability, and adaptivity to the underlying system resources. We propose a variant, post-local SGD that significantly improves the generalization performance of large batch sizes while reducing communication. Additionally, post-local SGD converges to flatter minima as opposed to large-batch methods, which can be understood by relating of local SGD to noise injection. Thus, local SGD is an enticing alternative to large-batch SGD.

1. Introduction

The workhorse training algorithm for most machine learning applications—including deep-learning—is stochastic gradient descent (SGD) (Robbins & Monro, 1985; Bottou, 2010). While vanilla SGD is a sequential algorithm, its mini-batch counterpart, which evaluates multiple stochastic gradients at the same time is the method of choice for modern distributed deep-learning applications. Mini-batch SGD offers three major advantages in view of parallelizability. Firstly,

it can exploit the compute parallelism locally available on modern computing devices such as GPUs, also allowing hierarchical parallelism. Secondly, it requires less frequent parameter updates which alleviates the communication bottleneck between the worker devices, which is crucial in a distributed setting, particularly for large models. Thirdly, the mini-batch size controls the noise in the gradients, and in turn controls variance reduction (Dekel et al., 2012). In the non-convex setting the noise effects how the optimization trajectory navigates the loss surface (Xing et al., 2018; Jastrz̄bski et al., 2017).

Recent applications (Goyal et al., 2017; You et al., 2017a) aim at reducing training time in the distributed setting by using many machines and running SGD with dramatically larger mini-batch size than reported previously in the literature. The impetus is to saturate local computation on a worker and reduce the total rounds of communication required. However, in practice these large-batch variants suffer from poor generalization, which takes away the gained computational advantage. The exact reason for this inefficiency is still not fully understood, but recent research has linked it to convergence to sharp minima (Keskar et al., 2016). While the theoretical benefit of flat minima is still debated (Dinh et al., 2017), many empirical studies show some degree of generalization benefits (Keskar et al., 2016; Yao et al., 2018). Additionally, as local parallelism is limited by memory constraints, large-batch variants must allow scaling to a large number of worker nodes. The resulting communication bottleneck (Keuper & Preundt, 2016; Lin et al., 2017) however severely limits scalability with the number of workers (e.g., Figure 8 in the Appendix).

To solve both presented core issues of large-batch SGD¹ i.e., (i) generalization, and (ii) scalability to a large number of workers, we propose to leverage novel variants of local SGD (McDonald et al., 2009; Zinkevich et al., 2010a; Zhang et al., 2016). Local SGD schemes update the parameters by averaging between the workers only after several local steps (without communication)—in contrast to mini-batch SGD that requires communication for each update step. We propose a novel local-SGD variant, referred to as post-local SGD, which uses frequent communication during the be-

¹School of computer and communication science, EPFL, Lausanne, Switzerland.

¹ Large-batch SGD refers to mini-batch SGD with large mini-batch size throughout this paper.

ginning of training but reduces it towards the end. Our algorithm is able to scale to dramatically larger batch sizes without accuracy loss. We also show that it converges to flatter minima, compared to large-batch SGD. Furthermore, we demonstrate that tuning the number of local steps between the communication rounds successfully decouples the two aspects of local parallelism and communication latency in local-SGD. This naturally leads to its hierarchical variant. The resulting training scheme leads to a significant decrease in the overall training time as well as improved scalability and robustness as the number of workers increases. Thus, we are able to alleviate both major problems with using large-batch SGD.

Our main contributions can be summarized as follows:

- This is the first work that empirically studies the trade-off in local SGD between communication efficiency (i.e., the number of workers and number of local steps) and expected SOTA accuracy. We provide guidelines for using local SGD in practice, highlighting success scenarios as well as current challenges.
- We propose a simple but very efficient training scheme, named post-local SGD, to address the current generalization issue of large-batch training. Large batches trained by post-local SGD enjoy significantly reduced communication cost while strongly outperforming most competing methods, for both small and large batch baselines. The local steps can be interpreted as a way of “injecting” structured stochastic noise to the optimization trajectory. Extensive empirical experiments verify that post-local SGD indeed generalizes to flatter minima.
- We propose a novel hierarchical extension of the local SGD training framework, further improving the adaptivity of local SGD to a wide range of real-world heterogeneous distributed systems.

2. Related Work

Local SGD and convergence theory. While mini-batch and parallel SGD are very well studied (Takáč et al., 2013; Zinkevich et al., 2010b), the theoretical understanding of local SGD variants is less clear. A parallel version of local SGD has been empirically studied in (Zhang et al., 2016). For a sub-class of convex models, Bijral et al. (2016) study local SGD in the setting of a general graph of workers. The theoretical convergence analysis has remained elusive for a long time, see e.g. Alistarh et al. (2018), until the very recent work of Stich (2018) which addresses the convergence rate in the convex case, and both Zhou & Cong (2018) and Yu et al. (2018) which address the non-convex case.

Large-batch training. State-of-the-art distributed deep learning frameworks (Abadi et al., 2016; Paszke et al., 2017; Seide & Agarwal, 2016) resort to synchronized large-batch SGD training, allowing scaling by adding more computational units and performing data-parallel synchronous SGD with mini-batches divided between devices. In order to improve the overall efficiency of mini-batch SGD training, those methods are restricted to increasing the batch size, while keeping the workload constant on each device. It has been shown that training with large batch size (e.g. batch size $> 10^3$ for the case of ImageNet) typically degrades the performance both in terms of training and test error (Chen & Huo, 2016; Li, 2017; Li et al., 2014; Keskar et al., 2016; Shallue et al., 2018; Defazio & Bottou, 2018).

Goyal et al. (2017) believe that this is an optimization problem and suggest performing a “learning rate warm-up” phase with linear scaling of the step-size. They are able to successfully train ImageNet with a ResNet-50 network and batch size 8K. On the other hand, Keskar et al. (2016); Hoffer et al. (2017); Jastrz̄bski et al. (2017) have all treated this as a generalization problem.

Generalization and Flat Minima Another line of related research links generalization to the flatness of minima. Keskar et al. (2016) empirically show that a larger batch size correlates with sharper minima, while Dinh et al. (2017) argue that current definitions of sharpness are problematic and a simple re-parametrization can make flat minima arbitrarily sharp and vice versa. In practice flatter minima are still preferred. Even if the sharp minima have the same training loss as the flat ones, small discrepancies of the data can easily lead to poor generalization performance (Hochreiter & Schmidhuber, 1997; Keskar et al., 2016; Yao et al., 2018).

Several works try to find flatter minima for better generalization performance. Chaudhari et al. (2016) propose entropy-SGD, which uses computationally intensive Langevin dynamics to bias SGD to flat regions of the “energy landscape”. The follow-up work (Chaudhari et al., 2017) combines entropy-SGD with elastic-SGD for the distributed training, which shows the better performance than mini-batch SGD at the same wall-clock time. However, it is unclear if it generalizes to flat minima, as a branch of newly introduced hyper-parameters and unclear experimental setup make it hard to reproduce the results. Wen et al. (2018) perform averaging over perturbed models to eliminate sharp minima, which requires to manually inject noise to the model and perform a de-noising step after the gradient computation. Izmailov et al. (2018) use cyclic learning rates along the trajectory of SGD and uniform averaging over the optimal model per cycle to get flatter minima and better generalization.

Generalization and Noise It is well known that mini-batch SGD traverses between vanilla SGD and GD in terms

of stochastic noise. It has also been argued that the poor performance of GD in non-convex problems can be improved by adding some isotropic white noise to the gradients, which helps it to escape poor local minima and avoid over-fitting (Neelakantan et al., 2015). However, Zhu et al. (2018); Xing et al. (2018) have reported that adding “structured” anisotropic noise, conditioned on the covariance of data, can outperform adding simple white noise on mini-batch SGD. Recently, Jastrzebski et al. (2017); Li et al. (2017); Mandt et al. (2017); Hu et al. (2017) have analyzed SGD through SDE (Stochastic Differential Equation) to explain its relationship with generalization. They investigate the dynamics of SGD, where the ratio of learning rate to batch size controls the magnitude of the noise and determines the flatness of the minima found by SGD. The importance of the scale of noise for non-convex optimization has also been studied in the Smith & Le (2018); Chaudhari & Soatto (2018).

3. Local SGD

We consider standard sum-structured optimization problems of the form $\min_{\mathbf{w} \in \mathbb{R}^d} \frac{1}{N} \sum_{i=1}^N f_i(\mathbf{w})$, where \mathbf{w} are the parameters of the model (e.g. the neural network), and f_i denotes the loss function of the i -th training data example.

The mini-batch update of SGD is given by,

$$\mathbf{w}_{t+1} := \mathbf{w}_t - \gamma_t \left[\frac{1}{|\mathcal{I}_t|} \sum_{i \in \mathcal{I}_t} \nabla f_i(\mathbf{w}_t) \right], \quad (1)$$

where $\mathcal{I}_t \subseteq [N]$ is a subset of indices of the N training datapoints, typically selected uniformly at random, and γ_t denotes the step-size (concrete values will be given below). $B := |\mathcal{I}_t|$ denotes the batch size, and the three update schemes of SGD, mini-batch SGD and GD respectively can be represented by $|\mathcal{I}_t| = 1$, $|\mathcal{I}_t| = B$ and $|\mathcal{I}_t| = N$. In the distributed setup, data examples are partitioned across K devices (such as GPUs or cloud compute nodes), each only having access to its local training data. The workhorse algorithm in this setting is again mini-batch SGD,

$$\mathbf{w}_{t+1} := \mathbf{w}_t - \gamma_t \left[\frac{1}{K|\mathcal{I}_t^k|} \sum_{k=1}^K \sum_{i \in \mathcal{I}_t^k} \nabla f_i(\mathbf{w}_t) \right], \quad (2)$$

where now the mini-batch of the k -th device is formed from local data \mathcal{I}_t^k , and the K devices compute gradients in parallel and then synchronize the local gradients by averaging. The global mini-batch size is defined as $B_{\text{glob}} = KB_{\text{loc}}$.

3.1. The Local SGD Algorithm

In contrast to mini-batch SGD, local SGD performs local sequential updates on each device, before aggregating the updates between the K devices, as illustrated in Figure 1.

Each worker k iteratively samples small mini-batches of fixed size B_{loc} , from its local data \mathcal{I}^k . It then sequentially

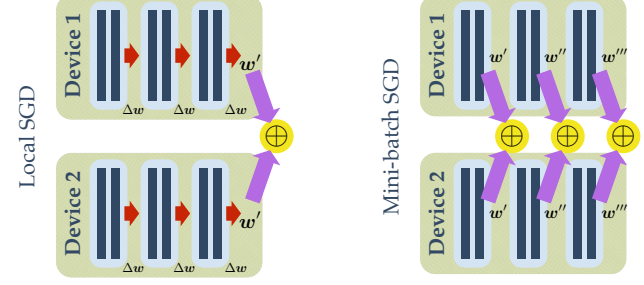


Figure 1. One round of local SGD (left) versus mini-batch SGD (right). In both settings $B_{\text{loc}} = 2$. For the local variant, the number of local steps is $H = 3$. Local parameter updates are depicted in red, whereas global averaging (synchronization) is depicted in purple.

performs $H \geq 1$ local parameter updates, before performing global parameter aggregation with the other devices.

Formally, one round of local SGD can be described as,

$$\mathbf{w}_{(t)+H}^k := \mathbf{w}_{(t)}^k - \sum_{h=1}^H \frac{\gamma_{(t)}}{B_{\text{loc}}} \cdot \sum_{i \in \mathcal{I}_{(t)+h-1}^k} \nabla f_i(\mathbf{w}_{(t)+h-1}^k), \quad (3)$$

where $\mathbf{w}_{(t)+h}^k$ denotes the local model on machine k after t global synchronization rounds and subsequent h local steps.

The definitions of $\gamma_{(t)}$ and $\mathcal{I}_{(t)+h-1}^k$ follow the same scheme.

After H local steps the synchronized global model $\mathbf{w}_{(t+1)}^k$ is obtained by averaging $\mathbf{w}_{(t)+H}^k$ among the K workers as in an all-reduce communication pattern

$$\mathbf{w}_{(t+1)}^k := \mathbf{w}_{(t)}^k - \frac{1}{K} \sum_{k=1}^K (\mathbf{w}_{(t)}^k - \mathbf{w}_{(t)+H}^k). \quad (4)$$

3.2. Convergence Theory of Local SGD

The main advantage of local SGD over mini-batch SGD is the drastic reduction in the amount of communication, when accessing the same number of data points or gradients. However, this advantage would be in vain if the convergence of local SGD were slower than that of mini-batch SGD. In the following section we therefore consider the theoretical convergence properties for local SGD.

First we discuss the convex setting. It is well-known that an individual run of SGD on a single machine converges as $\mathcal{O}((THB_{\text{loc}})^{-1})$, see e.g. Lacoste-Julien et al. (2012). By convexity, we can derive that averaging K instances of such local SGD executions will only improve the attained training objective value. However, this simple argument is not enough to quantify the speed-up of local SGD, i.e. it does not allow to incorporate a K -times reduction in the rate. This is still an active area of research (cf. also Alistarh et al. (2018); Stich (2018)). Stich (2018) very recently showed a linear speed-up, i.e. convergence at rate $\mathcal{O}((KTHB_{\text{loc}})^{-1})$

for strongly convex and smooth objective functions. Section B.2 in the Appendix experimentally illustrates the convergence properties of local SGD on the convex problem, for the different combination of H , K and B_{loc} .

Two recent theoretical contributions shed some light on local SGD in the non-convex setting. For smooth objective functions, Zhou & Cong (2018) show a rate $\mathcal{O}((KT B_{\text{loc}})^{-1/2})$ (for the decrement of the stochastic gradient) which only coincides in the extreme case $H = 1$ with the rate of mini-batch SGD. Yu et al. (2018) give an improved result $\mathcal{O}((HKT B_{\text{loc}})^{-1/2})$.

All these results assume a fixed communication frequency H . However, it is not clear yet whether this is the best choice in general. Intuitively, one would expect when the diversity of the local sequences $\mathbf{w}_{(t)+h}^k$ is small, for instance measured as $\frac{1}{K} \sum_{k=1}^K \mathbb{E} \|\bar{\mathbf{w}}_{(t)+h}^k - \mathbf{w}_{(t)+h}^k\|^2$ for $\bar{\mathbf{w}}_{(t)+h}^k := \frac{1}{K} \sum_{k=1}^K \mathbf{w}_{(t)+h}^k$; then one has to communicate less frequently. On the other hand when the difference between the sequences is larger (as expected in the beginning of the training process) then one should communicate updates more frequently. Zhang et al. (2016) empirically studied the effect of the averaging frequency on the quality of the solution for some problem cases. They observe that more frequent averaging at the beginning of the optimization can help and bring forward a theoretical illustration that supports this finding. Also Bijral et al. (2016) argue to average more frequently at the beginning. Thus, we will adopt such a strategy later in the experiments, while motivating post-local SGD.

Post-local SGD. We consider a variant of local SGD, named post-local SGD, which uses frequent communication during the first phase of training but reduces it towards the end. The next subsection further explains the benefits of using local steps from the aspect of stochastic noise, motivating our post-local SGD scheme.

3.3. Connecting Local SGD with Stochastic Noise

We study how local SGD can be interpreted as a method of injecting structured noise to gradients. Let us rewrite (2) as $\mathbf{w}_{t+1} = \mathbf{w}_t - \gamma \hat{\mathbf{g}}_t$ where $\hat{\mathbf{g}}_t := \frac{1}{B_{\text{glob}}} \sum_i \nabla f_i(\mathbf{w}_t)$ and γ_t is chosen to be the constant γ . Note that $\hat{\mathbf{g}}$ is an unbiased estimator of \mathbf{g}_t , i.e., $\mathbb{E} \hat{\mathbf{g}}_t = \mathbf{g}_t$.

Equation (2) can further be written as,

$$\begin{aligned} \mathbf{w}_{t+1} &= \mathbf{w}_t - \gamma \hat{\mathbf{g}}_t = \mathbf{w}_t - \gamma \mathbf{g}_t + \gamma(\hat{\mathbf{g}}_t - \mathbf{g}_t) \\ &= \mathbf{w}_t - \gamma \mathbf{g}_t + \gamma \epsilon, \end{aligned} \quad (5)$$

where $\epsilon := \mathbf{g}_t - \hat{\mathbf{g}}_t$ is approximately zero-mean Gaussian random noise (for most data-sets) with the variance $\Sigma(\mathbf{w})$. The variance matrix $\Sigma(\mathbf{w})$ following Hoffer et al. (2017); Hu et al. (2017), for uniform sampling of mini-batch indices (w/ or w/o replacement), can be approximated as

$$\Sigma(\mathbf{w}) \approx \left(\frac{1}{B_{\text{glob}}} - \frac{1}{N} \right) \left(\frac{1}{N} \sum_{i=1}^N \nabla f_i(\mathbf{w}) \nabla f_i(\mathbf{w})^\top \right). \quad (6)$$

Zhu et al. (2018); Jastrz̄bski et al. (2017); Mandt et al. (2017) interpret (5) as an Euler-Maruyama approximation to the SDE. In the underlying SDE and with the condition $B_{\text{glob}} \ll N$, the learning rate and the batch size only appear in the ratio $\frac{\gamma}{B_{\text{glob}}}$, controlling the stochastic noise sampled from $\Sigma(\mathbf{w})$. Jastrz̄bski et al. (2017) theoretically and experimentally support this claim, that constant $\frac{\gamma}{B_{\text{glob}}}$ controls the magnitude of stochastic noise which ensures wider minima and better generalization. It is also empirically verified by the success of ImageNet training (Goyal et al., 2017).

However, the generalization difficulty of large-batch training remains, as clearly illustrated in Figure 3 and Figure 4(b), as well as in Shallue et al. (2018); Defazio & Bottou (2018). We argue that the main reason behind this is the reduced noise magnitude, which comes from the break down of $\frac{\gamma}{B_{\text{glob}}}$ scaling for large batch size and smaller dataset size when $B_{\text{glob}} \ll N$ (Jastrz̄bski et al., 2017).

The proposed post-local SGD naturally addresses this generalization issue. Using fixed $\frac{\gamma}{B_{\text{glob}}}$ as mini-batch SGD, the dominant difference of local SGD training dynamics comes from the stochastic noise ϵ during the local update phase. The ϵ will be approximately sampled with the variance matrix $\frac{B_{\text{glob}}}{B_{\text{loc}}} \Sigma(\mathbf{w})$ instead of $\Sigma(\mathbf{w})$, causing the stochastic noise determined by H and K to increase.

In our setup, post-local SGD begins less frequent communication (i.e., $H > 1$) after performing the first learning rate decay², which is the phase corresponding to the turnover point of the model that gradually and eventually converges to the minima (Robbins & Monro, 1985; Smith et al., 2017). Given the positive effect of adding well-structured stochastic noise to SGD dynamics for non-convex problems (Smith & Le, 2018; Chaudhari & Soatto, 2018; Zhu et al., 2018; Xing et al., 2018), the communication efficient post-local SGD can generalize better and lead to flatter minima than mini-batch SGD.

3.4. Hierarchical Local SGD

Real world systems come with different communication bandwidths on several levels. In this scenario, we propose to employ local SGD on each level of the hierarchy, adapted

² In Appendix B.4.2 and C.1, we investigate the trade-off between the magnitude of the stochastic noise and the training stability. In Appendix B.4.2, we found that at the initial training phase and with a relatively large learning rate, the introduced stochastic noise is too large so as to worse the stability of the training and fall the difficulty of significantly improving the training performance. While in Appendix C.1, we further illustrate that performing post-local SGD after the first learning rate is sufficient and effective choice of escaping the sharp minima.

to each corresponding computation vs communication trade-off. The resulting scheme, hierarchical local SGD, offers significant benefits in system adaptivity and performance. Due to the space limitation, we refer to Appendix D for its algorithmic description and empirical evaluation.

4. Results

In this section we detail our experiments with local-SGD variants given in the previous section.

4.1. General Setup

Datasets. We use the following classification tasks.

- CIFAR-10/100 (Krizhevsky & Hinton, 2009). Each consist of a training set of 50K and a test set of 10K color images of 32×32 pixels, as well as 10 and 100 target classes respectively. We adopt the standard data augmentation scheme and preprocessing scheme (He et al., 2016a; Huang et al., 2016b).
- ImageNet (Russakovsky et al., 2015). The ILSVRC 2012 classification dataset consists of 1.28 million images for training, and 50K for validation, with 1K target classes. We use ImageNet-1k (Deng et al., 2009) and adopt the same data preprocessing and augmentation scheme as in (He et al., 2016a;b; Simonyan & Zisserman, 2014). The network input image is a 224×224 pixel random crop from augmented images, with per-pixel mean subtracted.

Models. We use ResNet-20 (He et al., 2016a) with CIFAR-10 as a base configuration to understand different properties of (post-)local SGD. We then empirical evaluate the large-batch training performance of (post-)local SGD, for ResNet-20, Densenet-40-12 (Huang et al., 2016a) and WideResNet-28-10 (Zagoruyko & Komodakis, 2016) on CIFAR-10/100. In the end, we use ResNet-50 (He et al., 2016a) on the challenging ImageNet to investigate the accuracy and scalability of (post-)local SGD training.

For the weight initialization we follow Goyal et al. (2017), where we adopt the initialization introduced by He et al. (2015) for convolution layers and initialize fully-connected layer from a zero-mean Gaussian distribution with the standard deviation of 0.01.

Implementation and platform. Our algorithm is implemented³ in PyTorch (Paszke et al., 2017), with a flexible configuration of the machine topology supported by Kubernetes. The cluster consists of 15 $2 \times$ Intel Xeon E5-2680 v3 servers and has 30 NVIDIA TITAN Xp GPUs in total. In the rest of the paper, we use $a \times b$ -GPU to denote the topology of the cluster, i.e., a nodes and each with b GPUs.

³ The code will be publicly available soon.

Specific learning tricks for large-batch SGD. We refer the tricks proposed recently for the efficient large batch training (Goyal et al., 2017), to “large-batch learning tricks”. The tricks are formalized by the following two configurations: (1) linearly scaling the learning rate w.r.t. the global mini-batch size; (2) gradually warm-up the learning rate from a small value. See Appendix A.3 for more details.

The distributed training procedure on CIFAR-10/100⁴.

The experiments follow the common mini-batch SGD training scheme for CIFAR (He et al., 2016a;b; Huang et al., 2016a) and all competing methods access the same total amount of data samples regardless of the number of local steps. The training procedure is terminated when the distributed algorithms have accessed the same number of samples as a standalone worker would access. For example, ResNet-20, Densenet-40-12 and WideResNet-28-10 would access 300, 300 and 250 epochs respectively. The data is partitioned among the GPUs and reshuffled globally every epoch. The local mini-batches are sampled among the local data available on each GPU, and its size B_{loc} is fixed to 128.

The learning rate scheme follows He et al. (2016a); Huang et al. (2016a), where we drop the initial learning rate by 10 when the model has accessed 50% and 75% of the total number of training samples. The initial learning rate is fine-tuned for each model and each task on the single GPU, and scaled by the global mini-batch size with large-batch learning tricks.

In addition to this, we use a Nesterov momentum of 0.9 without dampening, which is applied independently to each local model. For all architectures, following He et al. (2016a), we do not apply weight decay on the learnable Batch Normalization (BN) coefficients. For the BN for distributed training we again follow Goyal et al. (2017) and compute the BN statistics independently for each worker.

4.2. Experiments with Local SGD

Local SGD is an easy plug-in alternative for mini-batch SGD, with significantly improved communication efficiency and guaranteed performance for arbitrary dataset size. We empirically study local SGD training for the setup described above. The main findings and guidelines for using the algorithm are summarized below.

Significantly better scalability when increasing the number of workers on CIFAR, in terms of time-to-accuracy. Figure 2 demonstrates the speedup in time-to-accuracy for training ResNet-20 for CIFAR-10, with varying number of GPUs K from 1 to 16 and the number of local steps H from 1 to 16. $H = 1$ corresponds to the mini-batch SGD case. The communication is on top of an 8×2 -GPU cluster with 10 Gbps network bandwidth. The speedup in Figure 2 mea-

⁴ See Appendix A.4 for more details.

sures the inverse ratio of the training time on any number of GPUs versus the time on 1 GPU, to reach the top-1 test accuracy of CIFAR-10 of 91.2% (which was the accuracy reported in original ResNet paper (He et al., 2016a)). The test accuracy is evaluated each time when the distributed algorithm has accessed the complete training dataset.

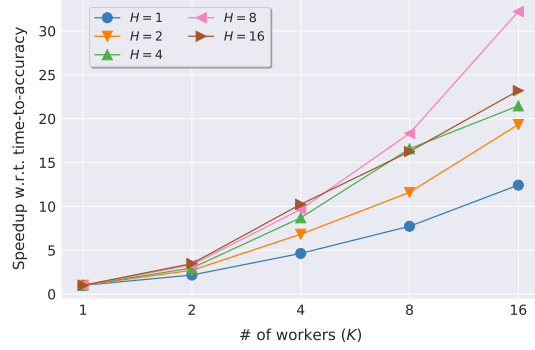


Figure 2. Scaling behavior of **local SGD** for increasing number of workers K , for different number of local steps H , for training **ResNet-20** on **CIFAR-10**. The reported **speedup** (averaged over three runs) is over single GPU training time for reaching the baseline top-1 test accuracy (91.2% as in the He et al. (2016a)). We use a 8×2 -GPU cluster with 10 Gbps network bandwidth. $H = 1$ is mini-batch SGD.

We demonstrate in Figure 2 that *local SGD scales 2 \times better than its mini-batch SGD counterpart, in terms of time-to-accuracy* under increasing the number of workers K . The benefits brought by local update steps H further show their advantages over the current large-batch training, where the current common large-batch SGD fixes the local mini-batch size B_{loc} and increases the number of workers K . The parallelism per device remains unchanged while facing the communication overhead. In this experiment, local SGD on 8 GPUs with $H = 8$ even achieves a 2 \times lower time-to-accuracy than mini-batch SGD with 16 GPUs. Moreover, the (near) linear scaling performance for $H = 8$ in Figure 2, shows that the main hyper-parameter H of local SGD is robust and consistently away from its mini-batch counterpart, under scaling the number of workers.

The effectiveness and success of scaling local SGD to even larger datasets (e.g., ImageNet) and larger clusters. Local SGD presents a competitive alternative to the current large-batch ImageNet training methods. Figure 10 in the Appendix B.3.1 shows that we can efficiently train state-of-the-art ResNet-50 (at least 1.5 \times speedup to reach 75% top-1 accuracy) for ImageNet (Goyal et al., 2017; You et al., 2017b) via local SGD on a 15×2 -GPU Kubernetes cluster.

4.2.1. GUIDELINES FOR USING LOCAL SGD

Empirical studies witness the efficiency and scalability of local SGD for different size of the dataset in Figure 2 and

Figure 10. However, for the training on a large-scale system, increasing the number of local steps H further to achieve even better communication efficiency is challenging. Figure 3 on CIFAR training presents some scenarios where local SGD has met a small quality drop when the number of local steps increased to the extreme value, e.g., $H = 16$ and $K = 16$.

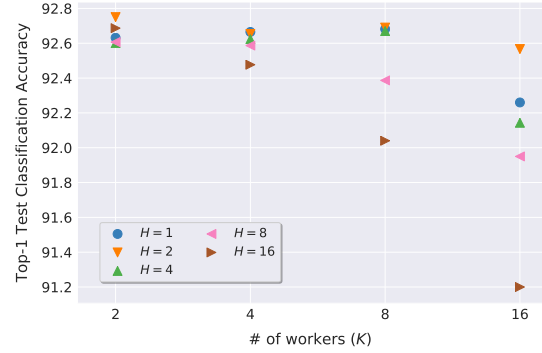


Figure 3. Top-1 test accuracy of training **ResNet-20** on **CIFAR-10**, under different K and H . All settings access to the same total number of training samples. $H = 1$ is mini-batch SGD. Results are averaged over three runs.

The challenge mentioned above also motivates a guideline (i.e., Figure 2 and Figure 3) for the practitioners w.r.t. the trade-off between communication efficiency and the best possible test accuracy. *Local SGD could always be a communication-efficient mini-batch SGD alternative for different practical pursuits.* For example, in terms of 92.26% test accuracy achieved by our mini-batch SGD implementation for $K = 16$, practitioners can either choose to achieve reasonable good training quality (91.2% as shown in He et al. (2016a)) with 2.59 \times speedup⁵ ($H = 8$) or get better performance (92.57%) with slightly reduced communication efficiency (1.76 \times speedup for $H = 2$).

Recently, Wang & Joshi (2018) propose to decrease local update steps H to guarantee the convergence, which is contrary to our theoretical understanding. Further, their evaluation (ResNet-50 on $K = 4$ with $B_{\text{glob}} = 512$) does not cover the difficult training scenarios of local SGD. For the same task (CIFAR-10) and K , our smaller ResNet-20 could reach a better accuracy with lesser communication⁶.

4.3. Experiments with Post-local SGD

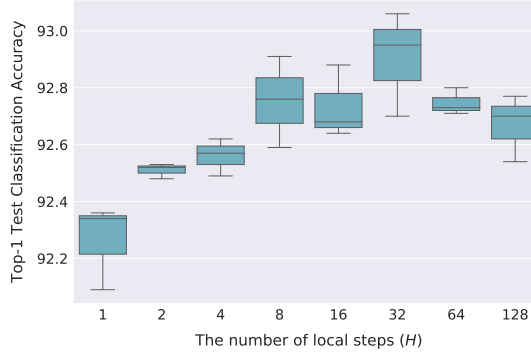
Section 3.3 connects local SGD as a way of injecting stochastic noise to the whole training procedure, and moti-

⁵ The speedup evaluated here is over the time-to-accuracy of mini-batch SGD.

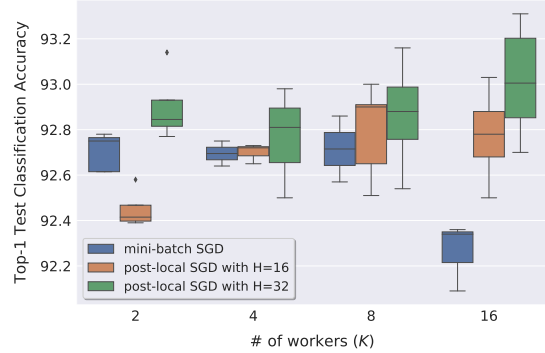
⁶ Some missing descriptions of Wang & Joshi (2018) make it hard to reproduce the results, so we had to directly compare with their reported value. The H in their paper forms a decreasing sequence from 10 while we use constant $H = 16$ over the training.

Table 1. Top-1 test accuracy of training different CNN models via **post-local SGD** on 16 GPUs with a large batch size ($B_{\text{glob}} = 2048$). $H = 1$ is mini-batch SGD. The reported results are the average of three runs. For the ease of comparison, we also include a “small batch baseline”, i.e., the accuracy of these models trained by mini-batch SGD with small batch size $B_{\text{glob}} = 256$. For more details, please refer to the Table 3 in the Appendix. We can witness that the accuracy of post-local SGD training (with large-batch) outperforms most of the fine-tuned baselines (either trained on small or large batch).

	CIFAR-10				CIFAR-100			
	small batch baseline	large batch ($H = 1$)	large batch ($H = 16$)	large batch ($H = 32$)	small batch baseline	large batch ($H = 1$)	large batch ($H = 16$)	large batch ($H = 32$)
ResNet-20	92.63 ± 0.26	92.26 ± 0.15	92.80 ± 0.16	93.02 ± 0.24	68.84 ± 0.06	68.30 ± 0.03	69.24 ± 0.26	69.38 ± 0.20
DenseNet-40-12	94.41 ± 0.14	94.03 ± 0.27	94.43 ± 0.12	94.58 ± 0.11	73.71 ± 0.14	73.36 ± 0.23	74.45 ± 0.30	75.03 ± 0.05
WideResNet-28-10	95.89 ± 0.10	95.10 ± 0.79	95.94 ± 0.06	95.76 ± 0.25	79.78 ± 0.16	79.32 ± 0.29	80.28 ± 0.13	80.65 ± 0.16

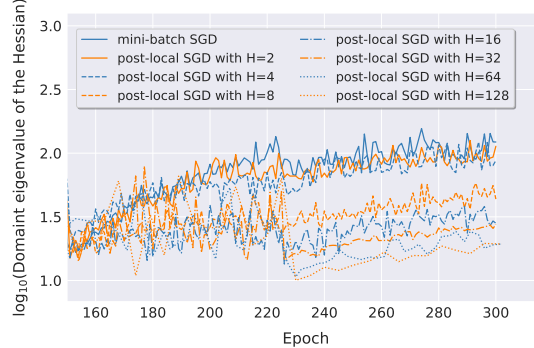


(a) The performance of post-local SGD for different number of local steps H on 16 GPUs. $H = 1$ is mini-batch SGD and $B_{\text{glob}} = 2048$.

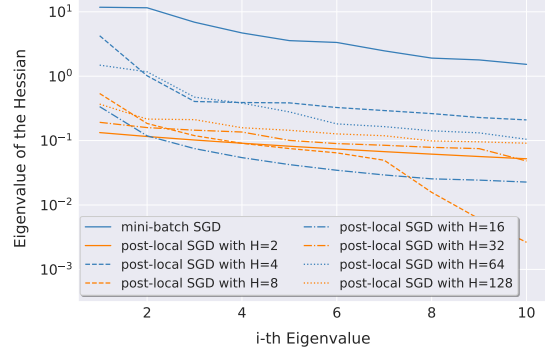


(b) The performance of post-local SGD for the different number of workers K for $H = 16$ and $H = 32$. The local batch size is fixed to $B_{\text{loc}} = 128$ and $B_{\text{glob}} = KB_{\text{loc}}$.

Figure 4. Top-1 test accuracy of training **ResNet-20** on **CIFAR-10**. The box-plot figures are derived from three runs.



(a) The dominant eigenvalue of the Hessian, which is evaluated on the test dataset per epoch. Only the phase related to the strategy of post-local SGD is visualized. Mini-batch SGD or post-local SGD with very much H (e.g., $H = 2, 4$) have noticeably larger dominant eigenvalue.



(b) Top 10 eigenvalues of the Hessian, which is evaluated on the test dataset for the best model of each training scheme. The top eigenvalues of the Hessian of the mini-batch SGD clearly present significant different pattern than the post-local SGD counterpart.

Figure 5. The spectrum of the Hessian for **ResNet-20** trained on **CIFAR-10**. The training is on top of $K = 16$ GPUs with $B_{\text{glob}} = 2048$. The spectrum is computed using power iteration (Martens & Sutskever, 2012; Yao et al., 2018) with the relative error of 1e-4. The top-1 test accuracy of mini-batch SGD is 92.57, while that of post-local SGD ranges from 92.33 to 93.07. Current large-batch trained with post-local SGD generalizes to solution with low curvature and with better generalization.

vates post-local SGD to address the generalization issue of large-batch SGD. Extensive empirical studies in this section confirm our theoretical understanding of post-local SGD and show that it indeed generalizes to flat minima with better test accuracy and significant communication benefits.

Post-local SGD generalizes better and faster than the mini-batch SGD. Table 1 summarizes the performance

of post-local SGD on large batch size ($B_{\text{glob}} = 2048$) across different architectures on CIFAR tasks for $H = 16$ and $H = 32$. Table 5 in the Appendix C.2 evaluates the speedup of training under the same setup. We can witness that post-SGD achieves at least $1.3 \times$ speedup over the whole training procedure compared to the mini-batch SGD counterpart, while enjoying the significantly improved generalization performance.

Figure C.5 in the Appendix demonstrates the generalization, scalability of post-local SGD for ImageNet training, where the post-local SGD outperforms mini-batch SGD baseline for both of $B_{\text{glob}} = 4096$ (76.18 and 75.87 respectively) and $B_{\text{glob}} = 8192$ (75.65 and 75.64 respectively) with $1.35\times$ speedup for the post-local SGD training phase. The benefits of post-local SGD training on ImageNet are even more pronounced when large-batch SGD meets the ineffectiveness phase (Shallue et al., 2018; Defazio & Bottou, 2018).

The effectiveness of post-local SGD training for different H and K . In Figure 4(a), applying any number of local steps over the case of large-batch training (when $B_{\text{glob}} = 2048$) improves the generalization performance compared to mini-batch SGD, where H controls the amount of increased stochastic noise. Figure 4(b) illustrates that post-local SGD is better than mini-batch SGD in general for different number of workers K and different B_{glob} . Mini-batch SGD might face the quality loss due to the generalization difficulty while post-local SGD presents consistent excellent generalization performance.

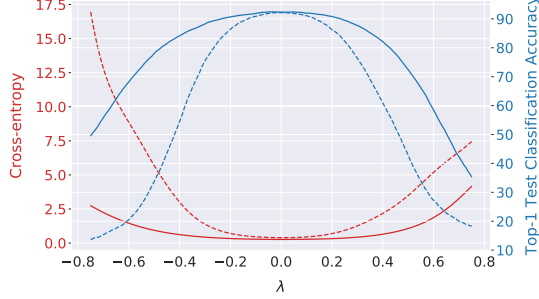
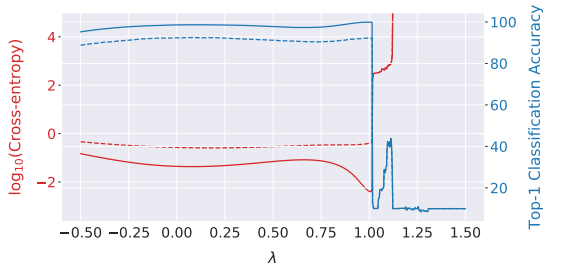
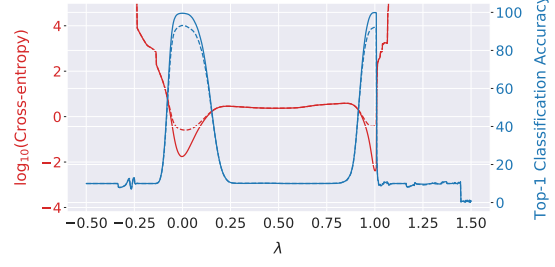


Figure 6. Sharpness visualization of the minima for **ResNet-20** trained on **CIFAR-10**. The training is on top of $K = 16$ GPUs with $B_{\text{glob}} = 2048$. The dashed lines are standard mini-batch SGD and the solid lines are post-local SGD with $H = 16$. The sharpness visualization of minima is performed via filter normalization (Li et al., 2018). The model is perturbed as $\mathbf{w} + \lambda \mathbf{d}$ by a shared random direction \mathbf{d} , and is evaluated by the whole dataset (training or test respectively). The top-1 test accuracy of mini-batch SGD is 92.25, while that of post-local SGD is 92.61. In the Appendix of Figure 15 we show the repeatability of the sharpness by using 10 random filter-normalized directions.

Post-local SGD generalizes to flatter minima than mini-batch SGD. Figure 5 evaluates the spectrum of the Hessian for mini-batch SGD and post-local SGD with different H , which again demonstrates the fact that large-batch SGD tends to stop at points with high Hessian spectrum while post-local SGD could easily generalize to a low curvature solution and with better generalization. Moreover, Figure 6 visualizes the sharpness of the model trained by different methods, and Figure 7 linearly interpolates two minima obtained by mini-batch SGD and post-local SGD. This underscores the goodness of post-local SGD.



(a) $\mathbf{w}_{\text{post-local SGD}}$ is trained with $H = 16$ and resumed from the checkpoint of $\mathbf{w}_{\text{mini-batch SGD}}$ before the first learning rate decay.



(b) $\mathbf{w}_{\text{post-local SGD}}$ is trained from scratch with $H = 16$.

Figure 7. 1-d linear interpolation between models $\mathbf{w}_{\text{post-local SGD}}$ and $\mathbf{w}_{\text{mini-batch SGD}}$, i.e., $\hat{\mathbf{w}} = \lambda \mathbf{w}_{\text{mini-batch SGD}} + (1 - \lambda) \mathbf{w}_{\text{post-local SGD}}$, for different minima of **ResNet-20** trained on **CIFAR-10**. The training is on top of $K = 16$ GPUs with $B_{\text{glob}} = 2048$. The solid lines correspond to evaluate $\hat{\mathbf{w}}$ on the whole training dataset while the dashed lines are on the test dataset. The post-local SGD in Figure 7(a) is trained from the checkpoint of $\mathbf{w}_{\text{mini-batch SGD}}$ before performing the first learning rate decay, while that of Figure 7(b) is trained from scratch. The top-1 test accuracy of mini-batch SGD is 92.25, while that of post-local SGD in Figure 7(a) and Figure 7(b) are 92.61 and 93.13 respectively. The interpolation is symmetric if we switch the position of $\mathbf{w}_{\text{post-local SGD}}$ and $\mathbf{w}_{\text{mini-batch SGD}}$, and we provide more cases of 1-d linear interpolation in the Appendix C.4.

5. Conclusion

In this work, we leverage the idea of local SGD for training in distributed and heterogeneous environments. We demonstrate its promise to alleviate the two major problems of current large-batch SGD methods: generalization and scalability to large number of workers. We show that local SGD variants can adapt to two crucial trade-offs in large scale learning: (i) convergence v/s communication and (ii) desirable noise v/s stability in non-convex optimization. We show that our novel variant of local SGD, post-local SGD, converges to flatter minima compared to traditional large-batch SGD, which partially explains its improved generalization performance. We also provide extensive experiments with several local-SGD variants, also including hierarchical local SGD, showing its adaptivity to available system resources. Overall, local-SGD comes off as a simpler but also more efficient algorithm, replacing complex ad-hoc tricks used for current large-batch SGD variants.

References

Abadi, M., Agarwal, A., Barham, P., Brevdo, E., Chen, Z., Citro, C., Corrado, G. S., Davis, A., Dean, J., Devin, M., et al. Tensorflow: Large-scale machine learning on heterogeneous distributed systems. *arXiv preprint arXiv:1603.04467*, 2016.

Alistarh, D., De Sa, C., and Konstantinov, N. The convergence of stochastic gradient descent in asynchronous shared memory. *arXiv*, March 2018.

Bijral, A. S., Sarwate, A. D., and Srebro, N. On data dependence in distributed stochastic optimization. *arXiv.org*, 2016.

Bottou, L. Large-scale machine learning with stochastic gradient descent. In Lechevallier, Y. and Saporta, G. (eds.), *COMPSTAT'2010 - Proceedings of the 19th International Conference on Computational Statistics*, pp. 177–187, 2010.

Chaudhari, P. and Soatto, S. Stochastic gradient descent performs variational inference, converges to limit cycles for deep networks. In *2018 Information Theory and Applications Workshop (ITA)*, pp. 1–10. IEEE, 2018.

Chaudhari, P., Choromanska, A., Soatto, S., LeCun, Y., Baldassi, C., Borgs, C., Chayes, J., Sagun, L., and Zecchina, R. Entropy-sgd: Biasing gradient descent into wide valleys. *arXiv preprint arXiv:1611.01838*, 2016.

Chaudhari, P., Baldassi, C., Zecchina, R., Soatto, S., Talwalkar, A., and Oberman, A. Parle: parallelizing stochastic gradient descent. *arXiv preprint arXiv:1707.00424*, 2017.

Chen, K. and Huo, Q. Scalable training of deep learning machines by incremental block training with intra-block parallel optimization and blockwise model-update filtering. In *Acoustics, Speech and Signal Processing (ICASSP), 2016 IEEE International Conference on*, pp. 5880–5884. IEEE, 2016.

Defazio, A. and Bottou, L. On the ineffectiveness of variance reduced optimization for deep learning. *arXiv preprint arXiv:1812.04529*, 2018.

Dekel, O., Gilad-Bachrach, R., Shamir, O., and Xiao, L. Optimal distributed online prediction using mini-batches. *Journal of Machine Learning Research*, 13(Jan):165–202, 2012.

Deng, J., Dong, W., Socher, R., Li, L.-J., Li, K., and Fei-Fei, L. ImageNet: A large-scale hierarchical image database. In *CVPR09*, 2009.

Dinh, L., Pascanu, R., Bengio, S., and Bengio, Y. Sharp minima can generalize for deep nets. *arXiv preprint arXiv:1703.04933*, 2017.

Goodfellow, I. J., Vinyals, O., and Saxe, A. M. Qualitatively characterizing neural network optimization problems. *arXiv preprint arXiv:1412.6544*, 2014.

Goyal, P., Dollár, P., Girshick, R., Noordhuis, P., Wesolowski, L., Kyrola, A., Tulloch, A., Jia, Y., and He, K. Accurate, large minibatch SGD: Training ImageNet in 1 hour. *arXiv preprint arXiv:1706.02677*, 2017.

Gropp, W., Lusk, E., and Skjellum, A. *Using MPI: portable parallel programming with the message-passing interface*, volume 1. MIT press, 1999.

He, K., Zhang, X., Ren, S., and Sun, J. Delving deep into rectifiers: Surpassing human-level performance on imagenet classification. In *Proceedings of the IEEE international conference on computer vision*, pp. 1026–1034, 2015.

He, K., Zhang, X., Ren, S., and Sun, J. Deep residual learning for image recognition. In *Proceedings of the IEEE Conference on Computer Vision and Pattern Recognition*, pp. 770–778, 2016a.

He, K., Zhang, X., Ren, S., and Sun, J. Identity mappings in deep residual networks. In *European Conference on Computer Vision*, pp. 630–645. Springer, 2016b.

Hochreiter, S. and Schmidhuber, J. . Flat minima. *Neural Computation*, 9(1):1–42, 1997.

Hoffer, E., Hubara, I., and Soudry, D. Train longer, generalize better: closing the generalization gap in large batch training of neural networks. *arXiv preprint arXiv:1705.08741*, 2017.

Hu, W., Li, C. J., Li, L., and Liu, J.-G. On the diffusion approximation of nonconvex stochastic gradient descent. *arXiv preprint arXiv:1705.07562*, 2017.

Huang, G., Liu, Z., Weinberger, K. Q., and van der Maaten, L. Densely connected convolutional networks. *arXiv preprint arXiv:1608.06993*, 2016a.

Huang, G., Sun, Y., Liu, Z., Sedra, D., and Weinberger, K. Q. Deep networks with stochastic depth. In *European Conference on Computer Vision*, pp. 646–661. Springer, 2016b.

Huang, G., Li, Y., Pleiss, G., Liu, Z., Hopcroft, J. E., and Weinberger, K. Q. Snapshot ensembles: Train 1, get m for free. *arXiv preprint arXiv:1704.00109*, 2017.

Izmailov, P., Podoprikin, D., Garipov, T., Vetrov, D., and Wilson, A. G. Averaging weights leads to wider optima and better generalization. *arXiv preprint arXiv:1803.05407*, 2018.

Jastrz̄bski, S., Kenton, Z., Arpit, D., Ballas, N., Fischer, A., Bengio, Y., and Storkey, A. Three factors influencing minima in sgd. *arXiv preprint arXiv:1711.04623*, 2017.

Keskar, N. S., Mudigere, D., Nocedal, J., Smelyanskiy, M., and Tang, P. T. P. On large-batch training for deep learning: Generalization gap and sharp minima. *arXiv preprint arXiv:1609.04836*, 2016.

Keuper, J. and Preundt, F.-J. Distributed training of deep neural networks: Theoretical and practical limits of parallel scalability. In *Proceedings of the Workshop on Machine Learning in High Performance Computing Environments*, pp. 19–26. IEEE Press, 2016.

Krizhevsky, A. and Hinton, G. Learning multiple layers of features from tiny images. 2009.

Lacoste-Julien, S., Schmidt, M., and Bach, F. A simpler approach to obtaining an $o(1/t)$ convergence rate for the projected stochastic subgradient method. *arXiv preprint arXiv:1212.2002*, 2012.

Li, H., Xu, Z., Taylor, G., Studer, C., and Goldstein, T. Visualizing the loss landscape of neural nets. In *Advances in Neural Information Processing Systems*, pp. 6391–6401, 2018.

Li, M. *Scaling distributed machine learning with system and algorithm co-design*. PhD thesis, Intel, 2017.

Li, M., Zhang, T., Chen, Y., and Smola, A. J. Efficient mini-batch training for stochastic optimization. In *Proceedings of the 20th ACM SIGKDD international conference on Knowledge discovery and data mining*, pp. 661–670. ACM, 2014.

Li, Q., Tai, C., et al. Stochastic modified equations and adaptive stochastic gradient algorithms. In *Proceedings of the 34th International Conference on Machine Learning-Volume 70*, pp. 2101–2110. JMLR. org, 2017.

Lin, Y., Han, S., Mao, H., Wang, Y., and Dally, W. J. Deep gradient compression: Reducing the communication bandwidth for distributed training. *arXiv preprint arXiv:1712.01887*, 2017.

Loshchilov, I. and Hutter, F. SGDR: stochastic gradient descent with restarts. *arXiv preprint arXiv:1608.03983*, 2016.

Mandt, S., Hoffman, M. D., and Blei, D. M. Stochastic gradient descent as approximate bayesian inference. *The Journal of Machine Learning Research*, 18(1):4873–4907, 2017.

Martens, J. and Sutskever, I. Training deep and recurrent networks with hessian-free optimization. In *Neural networks: Tricks of the trade*, pp. 479–535. Springer, 2012.

McDonald, R., Mohri, M., Silberman, N., Walker, D., and Mann, G. S. Efficient large-scale distributed training of conditional maximum entropy models. In Bengio, Y., Schuurmans, D., Lafferty, J. D., Williams, C. K. I., and Culotta, A. (eds.), *Advances in Neural Information Processing Systems 22*, pp. 1231–1239. Curran Associates, Inc., 2009.

Neelakantan, A., Vilnis, L., Le, Q. V., Sutskever, I., Kaiser, L., Kurach, K., and Martens, J. Adding gradient noise improves learning for very deep networks. *arXiv preprint arXiv:1511.06807*, 2015.

Paszke, A., Gross, S., Chintala, S., Chanan, G., Yang, E., DeVito, Z., Lin, Z., Desmaison, A., Antiga, L., and Lerer, A. Automatic differentiation in PyTorch. 2017.

Rabenseifner, R. Optimization of collective reduction operations. In *International Conference on Computational Science*, pp. 1–9. Springer, 2004.

Robbins, H. and Monro, S. A stochastic approximation method. In *Herbert Robbins Selected Papers*, pp. 102–109. Springer, 1985.

Russakovsky, O., Deng, J., Su, H., Krause, J., Satheesh, S., Ma, S., Huang, Z., Karpathy, A., Khosla, A., Bernstein, M., et al. Imagenet large scale visual recognition challenge. *International Journal of Computer Vision*, 115(3):211–252, 2015.

Seide, F. and Agarwal, A. CNTK: Microsoft's open-source deep-learning toolkit. In *Proceedings of the 22nd ACM SIGKDD International Conference on Knowledge Discovery and Data Mining*, pp. 2135–2135. ACM, 2016.

Shallue, C. J., Lee, J., Antognini, J., Sohl-Dickstein, J., Frostig, R., and Dahl, G. E. Measuring the effects of data parallelism on neural network training. *arXiv preprint arXiv:1811.03600*, 2018.

Simonyan, K. and Zisserman, A. Very deep convolutional networks for large-scale image recognition. *arXiv preprint arXiv:1409.1556*, 2014.

Smith, S. L. and Le, Q. V. A bayesian perspective on generalization and stochastic gradient descent. 2018.

Smith, S. L., Kindermans, P.-J., Ying, C., and Le, Q. V. Don't decay the learning rate, increase the batch size. *arXiv preprint arXiv:1711.00489*, 2017.

Stich, S. U. Local SGD converges fast and communicates little. *arXiv preprint arXiv:1805.09767*, 2018.

Takáč, M., Bijral, A., Richtárik, P., and Srebro, N. Mini-batch primal and dual methods for SVMs. In *ICML 2013 - Proceedings of the 30th International Conference on Machine Learning*, March 2013.

Thakur, R., Rabenseifner, R., and Gropp, W. Optimization of collective communication operations in MPICH. *The International Journal of High Performance Computing Applications*, 19(1):49–66, 2005.

Wang, J. and Joshi, G. Adaptive communication strategies to achieve the best error-runtime trade-off in local-update sgd. *arXiv preprint arXiv:1810.08313*, 2018.

Wen, W., Wang, Y., Yan, F., Xu, C., Chen, Y., and Li, H. Smoothout: Smoothing out sharp minima for generalization in large-batch deep learning. *arXiv preprint arXiv:1805.07898*, 2018.

Xing, C., Arpit, D., Tsirigotis, C., and Bengio, Y. A walk with sgd. *arxiv preprint arXiv:1802.08770*, 2018.

Yao, Z., Gholami, A., Lei, Q., Keutzer, K., and Mahoney, M. W. Hessian-based analysis of large batch training and robustness to adversaries. *arXiv preprint arXiv:1802.08241*, 2018.

You, Y., Zhang, Z., Demmel, J., Keutzer, K., and Hsieh, C.-J. ImageNet training in 24 minutes. *arXiv preprint arXiv:1709.05011*, 2017a.

You, Y., Zhang, Z., Hsieh, C.-J., and Demmel, J. 100-epoch ImageNet training with AlexNet in 24 minutes. *arXiv preprint arXiv:1709.05011*, 2017b.

Yu, H., Yang, S., and Zhu, S. Parallel restarted SGD for non-convex optimization with faster convergence and less communication. *arXiv preprint arXiv:1807.06629*, 2018.

Zagoruyko, S. and Komodakis, N. Wide residual networks. *arXiv preprint arXiv:1605.07146*, 2016.

Zhang, J., De Sa, C., Mitliagkas, I., and Ré, C. Parallel SGD: When does averaging help? *arXiv*, 2016.

Zhou, F. and Cong, G. On the convergence properties of a k-step averaging stochastic gradient descent algorithm for nonconvex optimization. In *Proceedings of the Twenty-Seventh International Joint Conference on Artificial Intelligence, IJCAI-18*, pp. 3219–3227. International Joint Conferences on Artificial Intelligence Organization, 7 2018. doi: 10.24963/ijcai.2018/447.

Zhu, Z., Wu, J., Yu, B., Wu, L., and Ma, J. The anisotropic noise in stochastic gradient descent: Its behavior of escaping from minima and regularization effects. 2018.

Zinkevich, M., Weimer, M., Li, L., and Smola, A. J. Parallelized stochastic gradient descent. In *Advances in neural information processing systems*, pp. 2595–2603, 2010a.

Zinkevich, M. A., Weimer, M., Smola, A. J., and Li, L. Parallelized stochastic gradient descent. *NIPS 2010: Advances in Neural Information Processing Systems 23*, pp. 1–37, 2010b.

A. Detailed Deep Learning Experimental Setup

A.1. Model Selection

Table 2. Scaling ratio for different models.

Model	Communication # parameters	Computation # flops per image	Computation/Communication scaling ratio
ResNet-20 (CIFAR-10)	0.27 million	0.041 billion	151.85
ResNet-20 (CIFAR-100)	0.27 million	0.041 billion	151.85
ResNet-50 (ImageNet-1k)	25.00 million	7.7 billion	308.00
DenseNet-40-12 (CIFAR-10)	1.06 million	0.28 billion	264.15
DenseNet-40-12 (CIFAR-100)	1.10 million	0.28 billion	254.55
WideResNet-28-10 (CIFAR-10)	36.48 million	5.24 billion	143.64
WideResNet-28-10 (CIFAR-100)	36.54 million	5.24 billion	143.40

The scaling ratio (You et al., 2017a) identifies the ratio between computation and communication, wherein DNN models, the computation is proportional to the number of floating point operations required for processing an input while the communication is proportional to model size (or the number of parameters).

Our local SGD training scheme will show more advantages over models with small “computation and communication scaling ratio”.

A.2. The Evaluation of Mini-batch SGD on Different Models and Datasets

Table 3 demonstrates an example that we can easily train state-of-the-art compute vision models through local SGD, with significantly reduced training time.

Table 3. The baseline performance of standard **mini-batch SGD** on different models for **CIFAR-10** and **CIFAR-100** (2×1 -GPU with $B_{loc} = 128$). Each model is trained from fine-tuned hyper-parameters, e.g., learning rate schedule, number of accessed samples.

	CIFAR-10		CIFAR-100	
	Test Top-1 Accuracy	Running Time (hour)	Test Top-1 Accuracy	Running Time (hour)
ResNet-20	92.63 ± 0.26	2.42	68.84 ± 0.06	2.47
DenseNet-40-12	94.41 ± 0.14	5.25	73.71 ± 0.14	5.27
WideResNet-28-10	95.89 ± 0.10	18.15	79.78 ± 0.16	19.08

A.3. Large Batch Learning Tricks

The work of (Goyal et al., 2017) proposes common configurations to tackle large-batch training for the ImageNet dataset. We specifically refer to their crucial techniques w.r.t. learning rate as “large batch learning tricks” in our main text. For a precise definition, this is formalized by the following two configurations:

- **Scaling the learning rate:** When the mini-batch size is multiplied by k , multiply the learning rate by k .
- **Learning rate gradual warm-up:** We gradually ramp up the learning rate from a small to a large value. In (our) experiments, with a large mini-batch of size kn , we start from a learning rate of η and increment it by a constant amount at each iteration such that it reaches $\hat{\eta} = k\eta$ after 5 epochs. More precisely, the incremental step size for each iteration is calculated from $\frac{\hat{\eta} - \eta}{5N/(K)}$, where N is the number of total training samples, K is the number of computing units and B_{loc} is the local mini-batch size.

A.4. The Hyperparameter Choices and Training Procedure, over Different Models/Datasets

A.4.1. CIFAR-10/CIFAR-100

The experiments follow the common mini-batch SGD training scheme for CIFAR (He et al., 2016a;b; Huang et al., 2016a) and all competing methods access the same total amount of data samples regardless of the number of local steps. The

training procedure is terminated when the distributed algorithms have accessed the same number of samples as a standalone worker would access. For example, ResNet-20, Densenet-40-12 and WideResNet-28-10 would access 300, 300 and 250 epochs respectively. The data is partitioned among the GPUs and reshuffled globally every epoch. The local mini-batches are then sampled among the local data available on each GPU, and its size is fixed to $B_{\text{loc}} = 128$.

The learning rate scheme follows [He et al. \(2016a\)](#); [Huang et al. \(2016a\)](#), where we drop the initial learning rate by 10 when the model has accessed 50% and 75% of the total number of training samples. The initial learning rates of ResNet-20, Densenet-40-12 and WideResNet-28-10 are fine-tuned on single GPU (which are 0.2, 0.2 and 0.1 respectively), and can be scaled by the global mini-batch size when using large-batch learning tricks.

In addition to this, we use a Nesterov momentum of 0.9 without dampening, which is applied independently to each local model. For all architectures, following [He et al. \(2016a\)](#), we do not apply weight decay on the learnable Batch Normalization (BN) coefficients. The weight decay of ResNet-20, Densenet-40-12 and WideResNet-28-10 are $1e-4$, $1e-4$ and $5e-4$ respectively. For the BN for distributed training we again follow [Goyal et al. \(2017\)](#) and compute the BN statistics independently for each worker.

Unless mentioned specifically, otherwise local SGD uses the exact same optimization scheme as mini-batch SGD.

A.4.2. IMAGENET

ResNet-50 training is limited to 90 passes over the data in total, and the data is disjointly partitioned and is re-shuffled globally every epoch. We adopt the large-batch learning tricks ([Goyal et al., 2017](#)) below. We linearly scale the learning rate based on # of GPUs $\times \frac{0.1}{256} \times B_{\text{glob}}$ where 0.1 and 256 is the base learning rate and mini-batch size respectively for standard single GPU training. The local mini-batch size is set to 128. For learning rate scaling, we perform gradual warmup for the first 5 epochs, and decay the scaled learning rate by the factor of 10 when local models have access 30, 60, 80 epochs of training samples respectively.

A.5. System Performance Evaluation

Figure 8 investigates the increased latency of transmitting data among CPU cores.

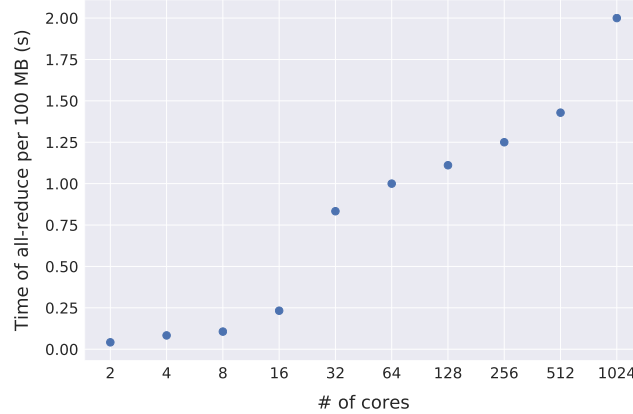


Figure 8. The data transmission cost (in seconds) of an all-reduce operation for 100 MB, over the different number of cores, using PyTorch's built-in MPI all-reduce operation. Each evaluation is the average result of 100 data transmissions on a Kubernetes cluster. The network bandwidth is 10 Gbps, and we use 48 cores per physical machine.

B. Local SGD

B.1. The Algorithm of Local SGD

Algorithm 1 Local SGD

input: the initial model $\mathbf{w}_{(0)}$;
input: training data with labels \mathcal{I} ;
input: mini-batch of size B_{loc} per local model;
input: step size η , and momentum m (optional);
input: number of synchronization steps T ;
input: number of local steps H ;
input: number of nodes K .

1: synchronize to have the same initial models $\mathbf{w}_{(0)} := \mathbf{w}_{(0)}$.
 2: **for all** $k := 1, \dots, K$ **do in parallel**
 3: **for** $t := 1, \dots, T$ **do**
 4: **for** $h := 1, \dots, H$ **do**
 5: sample a mini-batch from $\mathcal{I}_{(t)+h-1}^k$.
 6: compute the gradient

$$\mathbf{g}_{(t)+h-1}^k := \frac{1}{B_{\text{loc}}} \sum_{i \in \mathcal{I}_{(t)+h-1}^k} \nabla f_i(\mathbf{w}_{(t)+h-1}^k).$$
 7: update the local model to

$$\mathbf{w}_{(t)+h}^k := \mathbf{w}_{(t)+h-1}^k - \gamma_{(t)} \mathbf{g}_{(t)+h-1}^k.$$
 8: **end for**
 9: all-reduce aggregation of the gradients

$$\Delta_{(t)}^k := \mathbf{w}_{(t)}^k - \mathbf{w}_{(t)+H}^k.$$
 10: get new global (synchronized) model $\mathbf{w}_{(t+1)}^k$ for all K nodes:

$$\mathbf{w}_{(t+1)}^k := \mathbf{w}_{(t)}^k - \gamma_{(t)} \frac{1}{K} \sum_{i=1}^K \Delta_{(t)}^k$$
 11: **end for**
 12: **end for**

B.2. Numerical Illustration of Local SGD on a Convex Problem

In addition to our deep learning experiments, we first illustrate the convergence properties of local SGD on a small scale convex problem. For this, we consider logistic regression on the w8a dataset⁷ ($d = 300, n = 49749$). We measure the number of iterations to reach the target accuracy $\epsilon = 0.005$. For each combination of H, B_{loc} and K we determine the best learning rate by extensive grid search (cf. Section B.2.1 for the detailed experimental setup). In order to mitigate extraneous effects on the measured results, we here measure time in discrete units, that is we count the number of stochastic gradient computations and communication rounds, and assume that communication of the weights is $25 \times$ more expensive than a gradient computation, for ease of illustration.

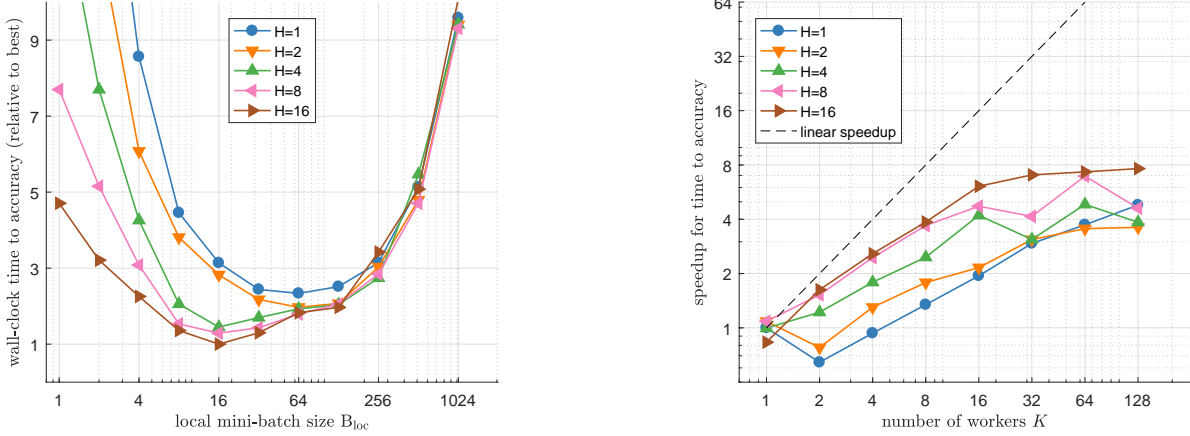
Figure 9(a) shows that different combinations of the parameters (B_{loc}, H) can impact the convergence time for $K = 16$. Here, local SGD with $(16, 16)$ converges more than $2 \times$ faster than for $(64, 1)$ and $3 \times$ faster than for $(256, 1)$.

Figure 9(b) depicts the speedup when increasing the number of workers K . Local SGD shows the best speedup for $H = 16$ on a small number of workers, while the advantage gradually diminishes for very large K .

B.2.1. EXPERIMENTAL SETUP FOR CONVEX EXPERIMENTS

For the illustrative experiments in Section B.2 we consider convergence of local SGD on the logistic regression problem, $f(\mathbf{w}) = \frac{1}{n} \sum_{i=1}^n \log(1 + \exp(-b_i \mathbf{a}_i^\top \mathbf{w})) + \frac{\lambda}{2} \|\mathbf{w}\|^2$, where $\mathbf{a}_i \in \mathbb{R}^d$ and $b_i \in \{-1, +1\}$ are the data samples, and regularization parameter $\lambda = 1/n$. For each run, we initialize $\mathbf{w}_0 = \mathbf{0}_d$ and measure the number of stochastic gradient evaluations (and communication rounds) until the best of last iterate and weighted average of the iterates reaches the target accuracy $f(\mathbf{w}_t) - f^* \leq \epsilon := 0.005$, with $f^* := 0.126433176216545$. For each configuration (K, H, B_{loc}) , we report the best result found with any of the following two stepsizes: $\gamma_t := \min(32, \frac{cn}{t+1})$ and $\gamma_t = 32c$. Here c is a parameter

⁷www.csie.ntu.edu.tw/~cjlin/libsvmtools/datasets/binary.html



(a) **Time** (relative to best method) to solve a regularized logistic regression problem to target accuracy $\epsilon = 0.005$ for $K = 16$ workers for $H \in 1, 2, 4, 8, 16$ and local mini-batch size B_{loc} . We simulate the network traffic under the assumption that communication is $25\times$ slower than a stochastic gradient computation.

(b) **Speedup** over the number of workers K to solve a regularized logistic regression problem to target accuracy $\epsilon = 0.005$, for $B_{loc} = 16$ and $H \in 1, 2, 4, 8, 16$. We simulate the network traffic under the assumption that communication is $25\times$ slower than a stochastic gradient computation.

Figure 9. Numerical illustration of local SGD on a convex problem.

that can take the values $c = 2^i$ for $i \in \mathbb{Z}$. For each stepsize we determine the best parameter c by a grid search, and consider parameter c optimal, if parameters $\{2^{-2}c, 2^{-1}c, 2c, 2^2c\}$ yield worse results (i.e. more iterations to reach the target accuracy).

B.3. More Results on Local SGD Training

B.3.1. TRAINING IMAGENET VIA LOCAL SGD

Figure 10 shows the effectiveness of scaling local SGD to the challenging ImageNet training. We limit ResNet-50 training to 90 passes over the data in total, and use the standard training configurations as mentioned in Appendix A.4.2.

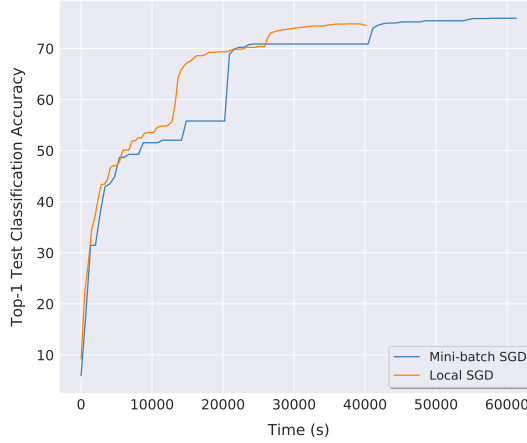


Figure 10. The performance of **local SGD** trained on **ImageNet-1k** with **ResNet-50** on a 15×2 -GPU cluster. We evaluate the model performance on test dataset after each complete accessing of the whole training samples. We apply the large-batch learning tricks (Goyal et al., 2017) to the ImageNet for these two methods. For local SGD, the number of local steps is set to $H = 8$.

Moreover, in our ImageNet experiment, the initial phase of local SGD training follows the theoretical assumption mentioned in Subsection 3.2, and thus we gradually warm up the number of local steps from 1 to the desired value H during the first few epochs of the training. We found that exponentially increasing the number of local steps from 1 by the factor of 2 (until reaching the expected number of local steps) performs well. For example, our ImageNet training uses $H = 8$, so the number of local steps for the first three epochs is 1, 2, 4 respectively.

B.3.2. LOCAL SGD SCALES TO LARGER BATCH THAN MINI-BATCH SGD

The empirical studies (Shallue et al., 2018; Defazio & Bottou, 2018) reveal the regime of maximal data parallelism across different tasks and models, where the large-batch training would reach the limit and additional parallelism provides no benefit whatsoever.

On contrary to standard large-batch training, *local SGD scales to larger batch size and provides additional parallelism upon the limitation of current large batch training*. Figure 11 shows the example of training ResNet-20 on CIFAR-10 with $H = 2$, which trains and generalizes better in terms of update steps while with reduced communication cost.

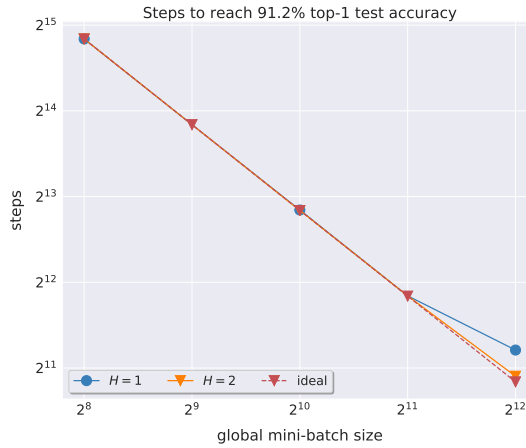


Figure 11. The relationship between steps to top-1 **test accuracy** and batch size, of training **ResNet-20** on **CIFAR-10**. The “step” is equivalent to the number of applying gradients. The B_{glob} is increased by adding more workers with fixed $B_{\text{loc}} = 128$. Results are averaged over three runs, each with fine-tuned learning rate.

B.4. Practical Attempts to Improve Standard Local SGD Training

We investigate different aspects of the training to address the quality when scaling local SGD to the extreme case, e.g., hybrid momentum scheme, warm up the local SGD or fine-tune the learning rate. In this section, we briefly present how these strategies are, and how they work in practice where we train ResNet-20 on CIFAR-10 on 16 GPUs.

B.4.1. WHEN LOCAL SGD MEETS MOMENTUM SCHEMES

Momentum mini-batch SGD is widely used in place of vanilla SGD. The distributed mini-batch SGD with vanilla momentum on K training nodes follows

$$\mathbf{u}_{(t)} = m\mathbf{u}_{(t-1)} + \frac{1}{K} \sum_{k=1}^K \nabla_{(t)}^k, \quad \mathbf{w}_{(t+1)} = \mathbf{w}_{(t)} - \gamma \mathbf{u}_{(t)}$$

where $\nabla_{(t)}^k = \frac{1}{|\mathcal{I}_{(t)}^k|} \sum_{i \in \mathcal{I}_{(t)}^k} \nabla f_i(\mathbf{w}_{(t)})$.

After H updates of mini-batch SGD, we have the following updated $\mathbf{w}_{(t+H)}$:

$$\mathbf{w}_{(t+H)} = \mathbf{w}_{(t)} - \gamma \left(\sum_{\tau=1}^H m^\tau \mathbf{u}_{(t-1)} + \sum_{\tau=0}^{H-1} \frac{m^\tau}{K} \sum_{k=1}^K \nabla_{(t)}^k + \dots + \sum_{\tau=0}^0 \frac{m^\tau}{K} \sum_{k=1}^K \nabla_{(t+H-1)}^k \right)$$

Coming back to the setting of local SGD, it is straightforward that we can apply momentum acceleration on each local model, or on global level (Chen & Huo, 2016). In the left of this section, we analyze the case of applying local momentum and global momentum. For ease of understanding, we assume the learning rate γ is the same throughout the H update steps.

Local SGD with Local Momentum. When applying local momentum on the local SGD, i.e., use independent identical momentum acceleration for each local model and only globally aggregate the gradients at the time $(t) + H$, we have the following local update scheme

$$\mathbf{u}_{(t)}^k = m\mathbf{u}_{(t-1)}^k + \nabla_{(t)}^k, \quad \mathbf{w}_{(t)+1}^k = \mathbf{w}_{(t)}^k - \gamma\mathbf{u}_{(t)}^k,$$

where $\nabla_{(t)}^k = \frac{1}{|\mathcal{I}_{(t)}^k|} \sum_{i \in \mathcal{I}_{(t)}^k} \nabla f_i(\mathbf{w}_{(t)})$. Consequently, after H local steps,

$$\mathbf{w}_{(t)+H}^k = \mathbf{w}_{(t)}^k - \gamma \left(\sum_{\tau=1}^H m^\tau \mathbf{u}_{(\tau-1)}^k + \sum_{\tau=0}^{H-1} m^\tau \nabla_{(\tau)}^k + \dots + \sum_{\tau=0}^0 m^\tau \nabla_{(t)+H-1}^k \right).$$

Substitute above equation to (4), we have

$$\begin{aligned} \mathbf{w}_{(t+1)} &= \mathbf{w}_{(t)} - \frac{1}{K} \sum_{k=1}^K \gamma \left(\sum_{\tau=1}^H m^\tau \mathbf{u}_{(\tau-1)}^k \sum_{\tau=0}^{H-1} m^\tau \nabla_{(\tau)}^k + \dots + \sum_{\tau=0}^0 m^\tau \nabla_{(t)+H-1}^k \right) \\ &= \mathbf{w}_{(t)} - \gamma \left(\sum_{\tau=1}^H \frac{m^\tau}{K} \sum_{k=1}^K \mathbf{u}_{(\tau-1)}^k + \sum_{\tau=0}^{H-1} m^\tau \left(\frac{1}{K} \sum_{k=1}^K \nabla_{(\tau)}^k \right) + \dots + \sum_{\tau=0}^0 \frac{m^\tau}{K} \sum_{k=1}^K \nabla_{(t)+H-1}^k \right) \end{aligned}$$

Compare the mini-batch SGD with local momentum local SGD after H update steps (H global update steps V.S. H local update steps and 1 global update step), we can witness that the main difference of these two update schemes is the difference between $\sum_{\tau=1}^H m^\tau \mathbf{u}_{(\tau-1)}$ and $\sum_{\tau=1}^H \frac{m^\tau}{K} \sum_{k=1}^K \mathbf{u}_{(\tau-1)}^k$, where mini-batch SGD hold a global $\mathbf{u}_{(t-1)}$ while each local model of the local SGD has their own $\mathbf{u}_{(t-1)}^k$. We will soon see the difference between the global momentum of mini-batch SGD and the local momentum of local SGD.

Local SGD with Global Momentum For global momentum local SGD, i.e., a more general variant of block momentum (Chen & Huo, 2016), we would like to only apply the momentum factor to the accumulated/synchronized gradients:

$$\begin{aligned} \mathbf{u}_{(t)} &= m\mathbf{u}_{(t-1)} + \frac{1}{\gamma} \sum_{k=1}^K \frac{1}{K} (\mathbf{w}_{(t)}^k - \mathbf{w}_{(t)+H}^k) = m\mathbf{u}_{(t-1)} + \frac{1}{\gamma} \sum_{k=1}^K \frac{1}{K} \sum_{l=0}^{H-1} \gamma \nabla_{(t)+l}^k, \\ \mathbf{w}_{(t+1)} &= \mathbf{w}_{(t)} - \gamma \mathbf{u}_{(t)} = \mathbf{w}_{(t)} - \gamma \left(m\mathbf{u}_{(t-1)} + \sum_{l=0}^{H-1} \sum_{k=1}^K \frac{1}{K} \nabla_{(t)+l}^k \right) \end{aligned}$$

where $\mathbf{w}_{(t)+H}^k = \mathbf{w}_{(t)}^k - \eta \sum_{l=0}^{H-1} \nabla_{(t)+l}^k = \mathbf{w}_{(t)}^k - \eta \sum_{l=0}^{H-1} \nabla_{(t)+l}^k$. Note that for local SGD, we consider summing the gradients from each local update, i.e., the model difference before and after one global synchronization, and then apply the global momentum to the gradients over workers over previous local update steps.

Obviously, there exists a significant difference between mini-batch momentum SGD and global momentum local SGD, at least the term $\sum_{\tau=0}^H m^\tau$ is canceled.

Local SGD with Hybrid Momentum. The following equation tries to combine local momentum with global momentum, which shows how the naive implementation of local momentum and global momentum will be.

First of all, based on the local momentum scheme, after H local update steps,

$$\mathbf{w}_{(t)+H}^k = \mathbf{w}_{(t)}^k - \gamma \left(\sum_{\tau=1}^H m^\tau \mathbf{u}_{(\tau-1)}^k + \sum_{\tau=0}^{H-1} m^\tau \nabla_{(\tau)}^k + \dots + \sum_{\tau=0}^0 m^\tau \nabla_{(t)+H-1}^k \right)$$

Together the result from local momentum with the global momentum, we have

$$\begin{aligned}
 \mathbf{u}_{(t)} &= m\mathbf{u}_{(t-1)} + \frac{1}{\gamma} \sum_{k=1}^K \frac{1}{K} (\mathbf{w}_{(t)}^k - \mathbf{w}_{(t)+H}^k) \\
 \mathbf{w}_{(t+1)} &= \mathbf{w}_{(t)} - \gamma \mathbf{u}_{(t)} = \mathbf{w}_{(t)} - \gamma \left[m\mathbf{u}_{(t-1)} + \frac{1}{\gamma} \sum_{k=1}^K \frac{1}{K} (\mathbf{w}_{(t)}^k - \mathbf{w}_{(t)+H}^k) \right] \\
 &= \mathbf{w}_{(t)} - \gamma \left[m\mathbf{u}_{(t-1)} + \sum_{\tau=1}^H \frac{m^\tau}{K} \sum_{k=1}^K \mathbf{u}_{(t-\tau)}^k + \sum_{\tau=0}^{H-1} \frac{m^\tau}{K} \sum_{k=1}^K \nabla_{(t)}^k + \dots + \sum_{\tau=0}^0 \frac{m^\tau}{K} \sum_{k=1}^K \nabla_{(t)+H-1}^k \right]
 \end{aligned}$$

where $\mathbf{u}_{(t-1)}$ is the global momentum memory and $\mathbf{u}_{(t-1)}$ is the local momentum memory for each node k .

Table 4. Evaluate local momentum and global momentum for **ResNet-20** on **CIFAR-10** data via local SGD training ($H = 1$ case) on 5×2 -GPU Kubernetes cluster. The local mini-batch size is 128 and base batch size is 64 (used for learning rate linear scale). Each local model will access to a disjoint data partition, using the standard learning rate scheme as [He et al. \(2016a\)](#).

local momentum	global momentum	test top-1
0.0	0.0	90.57
0.9	0.0	92.41
0.9	0.1	92.22
0.9	0.2	92.09
0.9	0.3	92.54
0.9	0.4	92.45
0.9	0.5	92.19
0.9	0.6	91.32
0.9	0.7	18.76
0.9	0.8	14.35
0.9	0.9	12.21
0.9	0.95	10.11

Local SGD with Momentum in Practice. In practice, it is possible to combine the local momentum with global momentum to further improve the model performance. For example, a toy example in Table 4 investigates the impact of different momentum schemes on CIFAR-10 trained with ResNet-20 on a 5×2 -GPU cluster, where some factors of global momentum could further slightly improve the final test accuracy.

However, the theoretical understanding of how local momentum and global momentum contribute to the optimization still remains unclear, which further increase the difficulty of tuning local SGD over H, K . An efficient way of using local and global momentum remains to be the further work and in this work, we only consider the local momentum.

B.4.2. WHEN LOCAL SGD WARMUP

We use the term “local step warm-up strategy”, to refer a specific variant of post-local SGD. More precisely, at the beginning of the training, the used number of local steps H will be gradually increased from 1 to the expected number of local steps H , by using different warm-up strategies. The warm-up strategies investigated here are “linear”, “exponential” and “constant”.

Please note that the implemented post-local SGD over the whole text only refers to the training scheme that uses frequent communication (i.e., $H = 1$) before the first learning rate decay and then reduce the communication frequency (i.e., $H > 1$) after the decay.

This section then investigates the trade-off between stochastic noise and the training stability. Also note that the Figure 3 in the main text has already presented one aspect of the trade-off. So the exploration below mainly focuses on the other aspect and tries to understand how will the scale of the added stochastic noise impact the training stability even the model has been stabilized to a region with good quality.

Figure 12 and Figure 13 investigate the potential improvement of using local step warm-up strategy for the case of training ResNet-20 on CIFAR-10. Figure 12 evaluates the warm-up strategy of “linear” and “constant” for different H , where the

evaluation of “exponential” warm-up strategy is omitted due to its close performance as “linear” warm-up. However, none of them really works well. Figure 13 further studies how the period of warm-up impacts the training performance, for the warm-up strategy like “linear”, “exponential” and “constant”. We can witness that even we increase the warm-up phase to 50 epochs where the training curve of mini-batch SGD becomes stabilized, the large noise introduced by the local SGD will soon degrade the status of training and lead to potential quality loss, as in Figure 13(a).

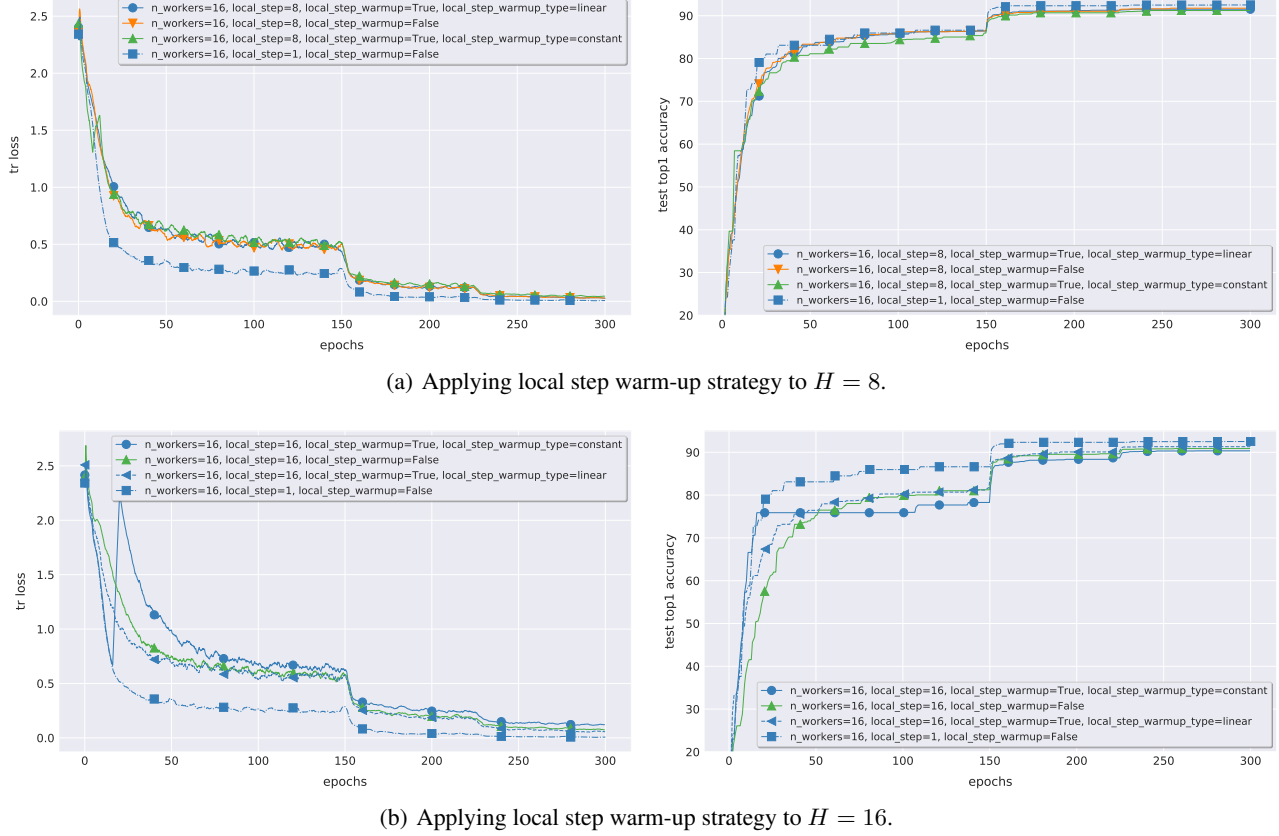
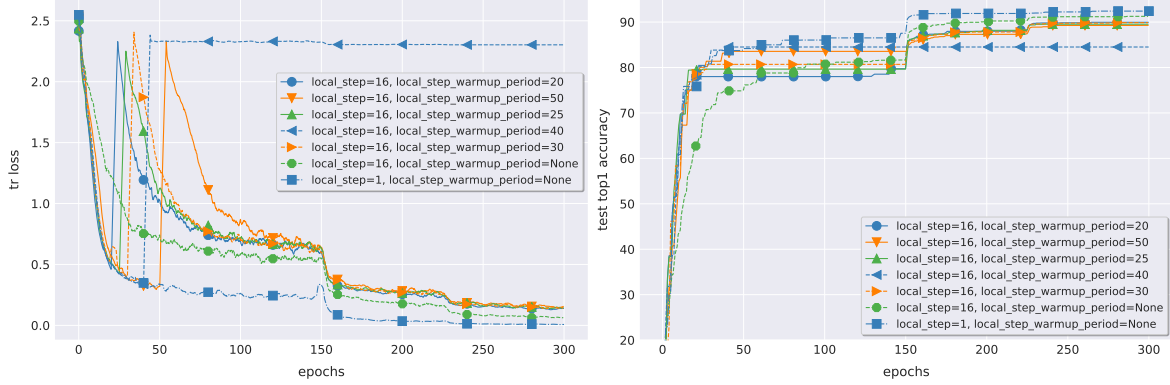
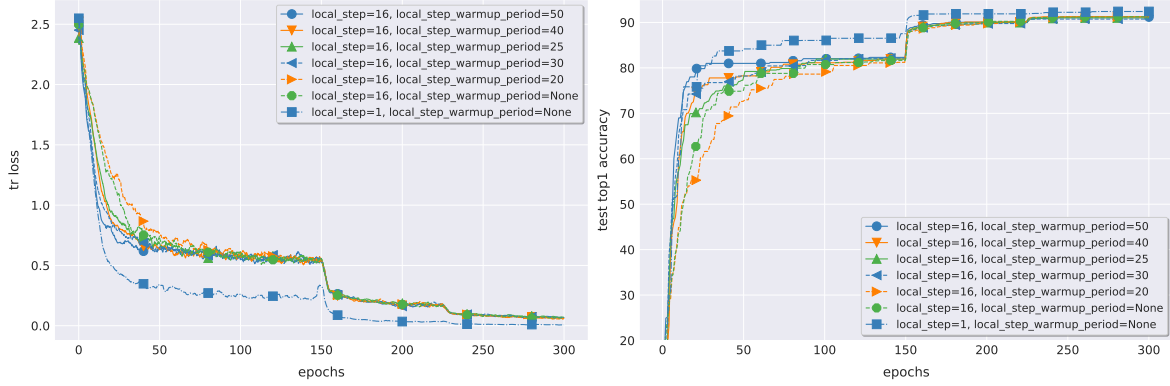


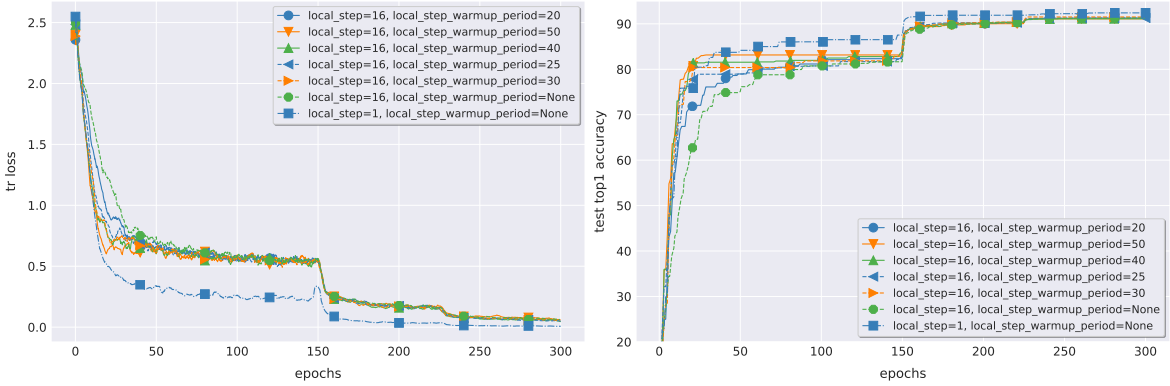
Figure 12. Investigate how local step warm-up strategy impacts the performance of training **CIFAR-10** with **ResNet-20** via **local SGD** (8×2 -GPU). The local batch size B_{loc} is fixed to 128. The warmup strategies are “linear” and “constant”, and the warm-up period used here is equivalent to the number of local steps H .



(a) Evaluate the impact of “constant” local step warm-up for different period of warm-up phase.



(b) Evaluate the impact of “linear” local step warm-up for different period of warm-up phase.



(c) Evaluate the impact of “exponential” local step warm-up for different period of warm-up phase.

Figure 13. Investigate how different warm-up period of the local step warm-up impacts the performance of training **CIFAR-10** with **ResNet-20** via **local SGD** (8×2 -GPU). The local batch size B_{loc} is fixed to 128, and the strategies to warm-up the number of local steps H are “linear”, “exponential” and “constant”.

C. Post-local SGD Training

C.1. The Effectiveness of Turning on Post-local SGD after the First Learning Rate Decay

In Figure 14, we study the sufficiency as well as the necessary of “injecting” more stochastic noise (i.e., using post-local SGD) into the optimization procedure after performing the first learning rate decay. Otherwise, the delayed noise injection (i.e., starting the post-local SGD only from the second learning rate decay) not only introduces more communication cost but also meets the increased risk of converging to sharper minima.

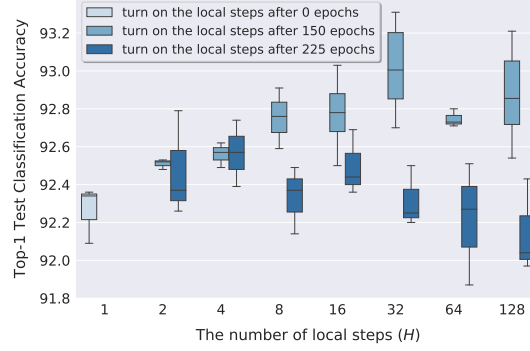


Figure 14. The effectiveness and necessary of turning on the post-local SGD after the first learning rate decay. The example here trains ResNet-20 on CIFAR-10 on 16 GPUs with $B_{\text{glob}} = 2048$.

C.2. The Speedup of Post-local SGD Training on CIFAR

Table 5. The **Speedup** of mini-batch SGD and post-local SGD, over different CNN models and datasets. The speedup is evaluated by $\frac{T_a}{T_a^K}$, where T_a is the training time of the algorithm a on 1 GPU and T_a^K corresponds to the training on K GPUs. We use 16 GPUs in total on an 8×2 -GPU cluster with 10 Gbps network bandwidth. The experimental setup is the same as Table 1.

	CIFAR-10			CIFAR-100		
	H=1	H=16	H=32	H=1	H=16	H=32
ResNet-20	9.45	12.24	13.00	8.75	11.05	11.67
DenseNet-40-12	8.31	10.80	11.37	8.04	10.59	10.85
WideResNet-28-12	5.33	7.94	8.19	5.29	7.83	8.14

Table 6. The **Speedup** of mini-batch SGD and post-local SGD (only consider the phase of performing post-local SGD) over different CNN models and datasets. The speedup is evaluated by $\frac{T_a}{T_a^K}$, where T_a is the training time of the algorithm a (corresponding to the second phase) on 1 GPU and T_a^K corresponds to the training on K GPUs. We use 16 GPUs in total on an 8×2 -GPU cluster with 10 Gbps network bandwidth. The experimental setup is the same as Table 1.

	CIFAR-10			CIFAR-100		
	H=1	H=16	H=32	H=1	H=16	H=32
ResNet-20	9.45	17.33	20.80	8.75	15.00	17.50
DenseNet-40-12	8.31	15.43	18.00	8.04	15.50	16.69
WideResNet-28-12	5.33	15.52	17.66	5.29	15.09	17.69

C.3. The Reproducibility of the Sharpness Visualization

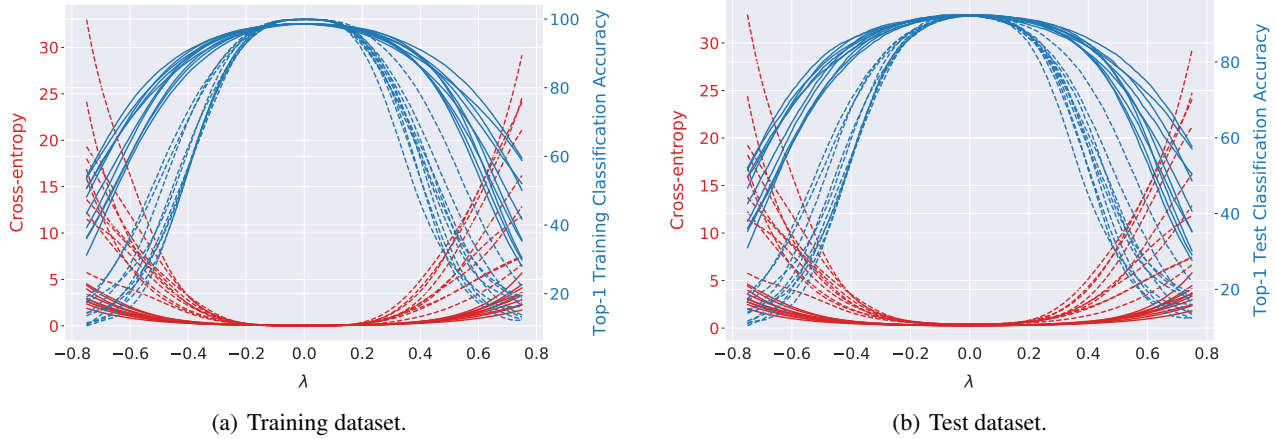


Figure 15. Sharpness visualization of the minima for **ResNet-20** trained on **CIFAR-10**. The training is on top of $K = 16$ GPUs and the local batch size is fixed to $B_{\text{loc}} = 128$. The dashed lines are standard mini-batch SGD and the solid lines are post-local SGD with $H = 16$. The sharpness visualization of minima is performed via filter normalization (Li et al., 2018). The model is perturbed as $\mathbf{w} + \lambda \mathbf{d}$ by a shared random direction \mathbf{d} , and is evaluated by the whole dataset (training or test respectively). The top-1 test accuracy of mini-batch SGD is 92.25, while that of post-local SGD is 92.61. The sharpness of these two minima is consistent over 10 different random directions.

C.4. 1-d linear interpolation between Models

The 1-d linear interpolation was taken by Goodfellow et al. (2014) and then widely used to study the “sharpness” and “flatness” of different minima (Keskar et al., 2016; Dinh et al., 2017; Li et al., 2018). In Figure 16 shown below, model trained by post-local SGD $\mathbf{w}_{\text{post-local SGD}}$ can generalize to flatter minima than that of mini-batch SGD $\mathbf{w}_{\text{mini-batch SGD}}$, either $\mathbf{w}_{\text{post-local SGD}}$ is trained from scratch, or resumed from the checkpoint of $\mathbf{w}_{\text{mini-batch SGD}}$ (i.e., the checkpoint is one-epoch ahead of the first learning rate decay so as to share the common weight structure with $\mathbf{w}_{\text{mini-batch SGD}}$).

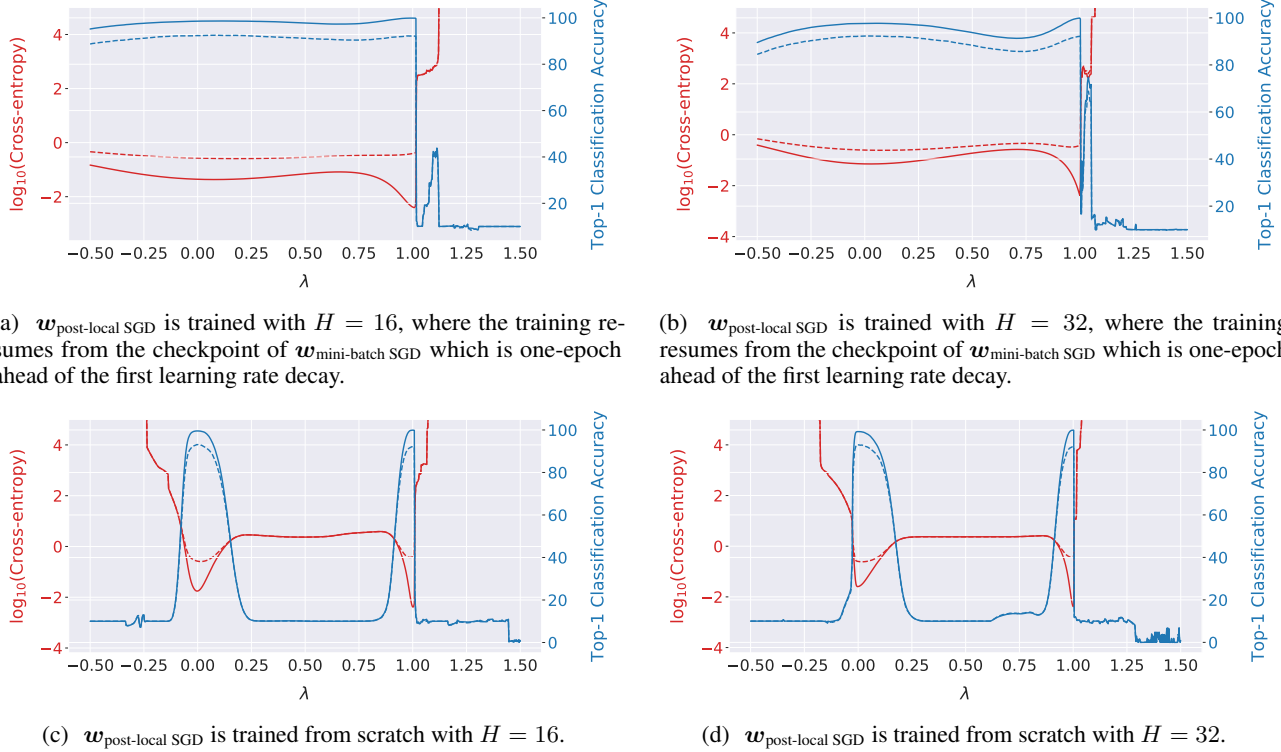
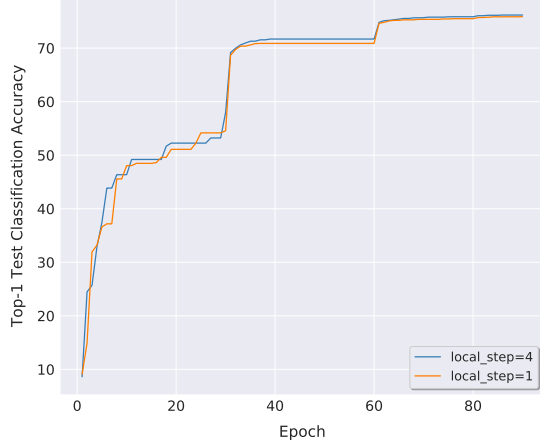


Figure 16. 1-d linear interpolation between models $\mathbf{w}_{\text{post-local SGD}}$ and $\mathbf{w}_{\text{mini-batch SGD}}$, i.e., $\hat{\mathbf{w}} = \lambda \mathbf{w}_{\text{mini-batch SGD}} + (1 - \lambda) \mathbf{w}_{\text{post-local SGD}}$, for different minima of **ResNet-20** trained on **CIFAR-10**. The training is on top of $K = 16$ GPUs and the local batch size is fixed to $B_{\text{loc}} = 128$. The solid lines correspond to evaluate $\hat{\mathbf{w}}$ on the whole training dataset while the dashed lines are on the test dataset. The post-local SGD in Figure 16(a) and Figure 16(d) is trained from the checkpoint of $\mathbf{w}_{\text{mini-batch SGD}}$ before performing the first learning rate decay, while that of Figure 16(c) and Figure 16(d) is trained from scratch. The top-1 test accuracy of mini-batch SGD is 92.25, while that of post-local SGD in Figure 16(a), Figure 16(b), Figure 16(c) and Figure 16(d), are 92.61, 92.35, 93.13 and 93.04 respectively.

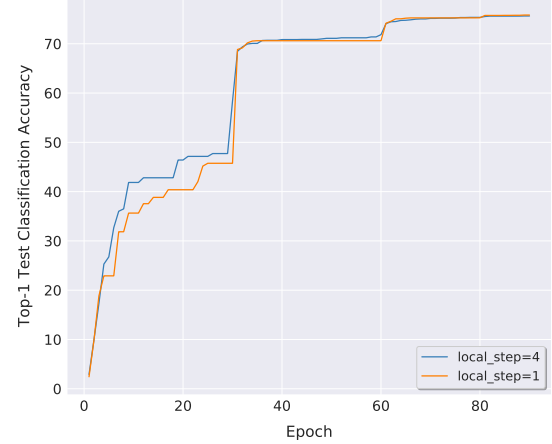
C.5. Post-local SGD Training on ImageNet

We evaluate the performance of post-local SGD on the challenging ImageNet training. Again we limit ResNet-50 training to 90 passes over the data in total, and use the standard training configurations as mentioned in Appendix A.4.2. The post-local SGD begins when performing the first learning rate decay.

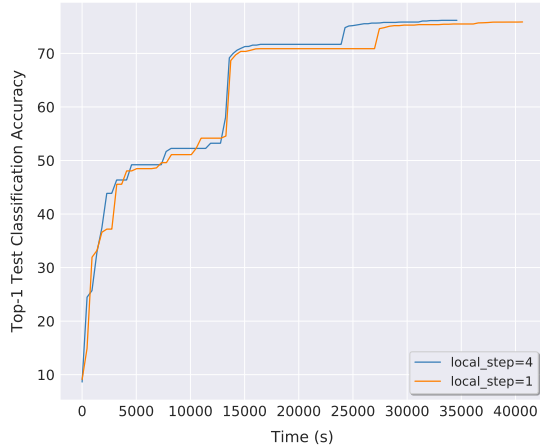
We can witness that post-local SGD outperforms mini-batch SGD baseline for both of $B_{\text{glob}} = 4096$ (76.18 and 75.87 respectively) and $B_{\text{glob}} = 8192$ (75.65 and 75.64 respectively).



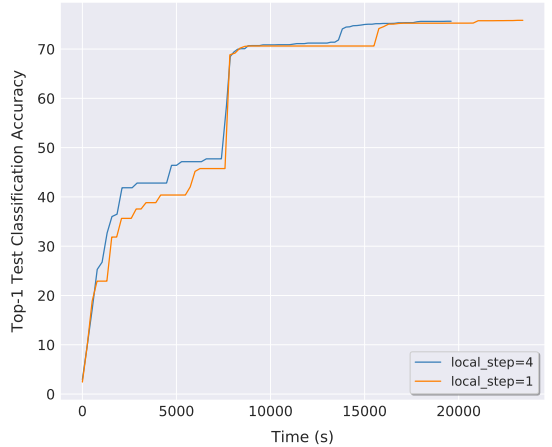
(a) The performance of post-local SGD training for **ImageNet-1k** with $B_{\text{glob}} = 4096$, in terms of epoch-to-accuracy.



(b) The performance of post-local SGD training for **ImageNet-1k** with $B_{\text{glob}} = 8192$, in terms of epoch-to-accuracy.



(c) The performance of post-local SGD training for **ImageNet-1k** with $B_{\text{glob}} = 4096$, in terms of time-to-accuracy.



(d) The performance of post-local SGD training for **ImageNet-1k** with $B_{\text{glob}} = 8192$, in terms of time-to-accuracy.

Figure 17. The performance of **post-local SGD** training for **ImageNet-1k**. We evaluate the model performance on test dataset after each complete accessing of the whole training samples. Note that due to the resource limitation of the main experimental platform in the paper, this set of experiments are on top of a 8×4 -GPU (V100) Kubernetes cluster with 10 Gbps network bandwidth.

D. Hierarchical Local SGD

The idea of local SGD can be leveraged to the more general setting of training on decentralized and heterogeneous systems, which is an increasingly important application area. Such systems have become common in the industry, e.g. with GPUs or other accelerators grouped hierarchically within machines, racks or even at the level of several data-centers. Hierarchical system architectures such as in Figure 18 motivate our hierarchical extension of local SGD. Moreover, end-user devices such as mobile phones form huge heterogeneous networks, where the benefits of efficient distributed and data-local training of machine learning models promises strong benefits in terms of data privacy.

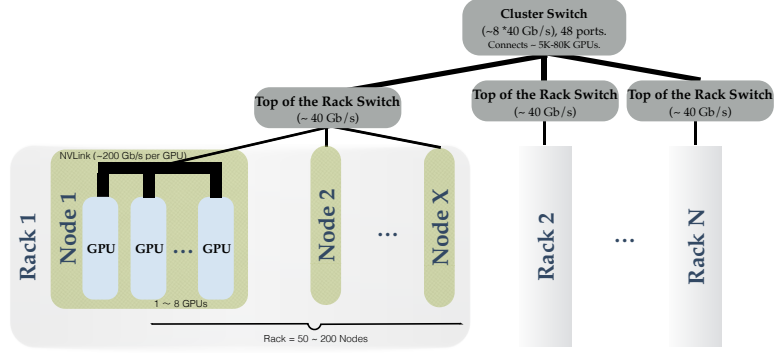


Figure 18. Illustration of a hierarchical network architecture of a cluster in the data center. While GPUs within each node are linked with fast connections (e.g. NVLink), connections between the servers within and between different racks have much lower bandwidth and latency (via top-of-the-rack switches and cluster switches). The hierarchy can be extended several layers further and further. Finally, edge switches face the external network at even lower bandwidth.

D.1. The Illustration of Hierarchical Local SGD

Real world systems come with different communication bandwidths on several levels. In this scenario, we propose to employ local SGD on each level of the hierarchy, adapted to each corresponding computation vs communication trade-off. The resulting scheme, hierarchical local SGD, offers significant benefits in system adaptivity and performance as we will see in the rest of the paper.

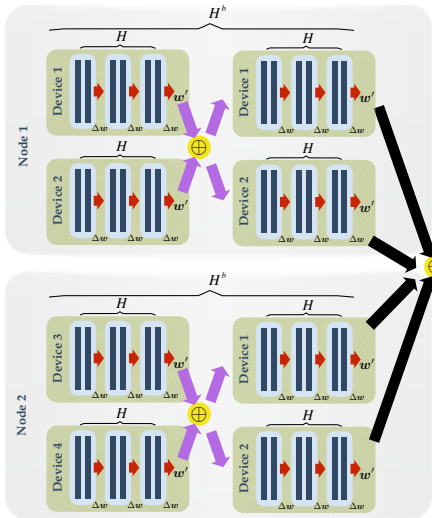


Figure 19. An illustration of hierarchical local SGD, for $B_{loc} = 2$, using the number of local steps $H = 3$ and the number of block steps $H^b = 2$. Local parameter updates are depicted in red, whereas block and global synchronization is depicted in purple and black respectively.

As the guiding example, we consider compute clusters which typically allocate a large number of GPUs grouped over several machines, and refer to each group as a GPU-block. Hierarchical local SGD continuously updates the local models on each GPU for a number of H *local update steps* before a (fast) synchronization within a GPU-block. On the outer level, after H^b such *block update steps*, a (slower) global synchronization over all GPU-blocks is performed. Figure 19 and Algorithm 2 depict how the hierarchical local SGD works, and the complete procedure is formalized below:

$$\begin{aligned}
 \mathbf{w}_{[(t)+l]+H}^k &:= \mathbf{w}_{[(t)+l]}^k - \sum_{h=1}^H \frac{\gamma_{[(t)]}}{B_{\text{loc}}} \cdot \sum_{i \in \mathcal{I}_{[(t)+l]+h-1}^k} \nabla f_i(\mathbf{w}_{[(t)+l]+h-1}^k) \\
 \mathbf{w}_{[(t)+l+1]}^k &:= \mathbf{w}_{[(t)+l]}^k - \frac{1}{K_i} \sum_{k=1}^{K_i} (\mathbf{w}_{[(t)+l]}^k - \mathbf{w}_{[(t)+l]+H}^k) \\
 \mathbf{w}_{[(t+1)]}^k &:= \mathbf{w}_{[(t)]}^k - \frac{1}{K} \sum_{k=1}^K (\mathbf{w}_{[(t)]}^k - \mathbf{w}_{[(t)+H^b]}^k)
 \end{aligned} \tag{7}$$

where $\mathbf{w}_{[(t)+l]+H}^k$ indicates the model after l block update steps and H local update steps, and K_i is the number of GPUs on the GPU-block i . The definition of $\gamma_{[(t)]}$ and $\mathcal{I}_{[(t)+l]+h-1}^k$ follows a similar scheme.

As the number of devices grows to the thousands (Goyal et al., 2017; You et al., 2017a), the difference between ‘within’ and ‘between’ block communication efficiency becomes more drastic. Thus, the performance benefits of our adaptive scheme compared to flat & large mini-batch SGD will be even more pronounced.

D.2. The Algorithm of Hierarchical Local SGD

Algorithm 2 Hierarchical Local SGD

input: the initial model $\mathbf{w}_{[(0)]}$;

input: training data with labels \mathcal{I} ;

input: mini-batch of size B_{loc} per local model;

input: step size η , and momentum m (optional);

input: number of synchronization steps T over nodes;

input: number of local update steps H ;

input: number of block update steps H^b ;

input: number of nodes K in total;

input: number of nodes K' per GPU-block.

1: synchronize to have the same initial models $\mathbf{w}_{[(0)]} := \mathbf{w}_{[(0)]}$.

2: **for all** $k := 1, \dots, K$ **do in parallel**

3: **for** $t := 1, \dots, T$ **do**

4: **for** $l := 1, \dots, H^b$ **do**

5: **for** $h := 1, \dots, H$ **do**

6: sample a mini-batch from $\mathcal{I}_{[(t)+l]+h-1}^k$.

7: compute the gradient

$$\mathbf{g}_{[(t)+l]+h-1}^k := \frac{1}{B_{\text{loc}}} \sum_{i \in \mathcal{I}_{[(t)+l]+h-1}^k} \nabla f_i(\mathbf{w}_{[(t)+l]+h-1}^k).$$

8: update the local model

$$\mathbf{w}_{[(t)+l]+h}^k := \mathbf{w}_{[(t)+l]+h-1}^k - \gamma_{[(t)]} \mathbf{g}_{[(t)+l]+h-1}^k.$$

9: **end for**

10: all-reduce aggregation of the gradients

$$\Delta_{[(t)+l]}^k := \mathbf{w}_{[(t)+l]}^k - \mathbf{w}_{[(t)+l]+H}^k.$$

11: get new block (synchronized) model $\mathbf{w}_{[(t)+l+1]}^k$ for K' block nodes:

$$\mathbf{w}_{[(t)+l+1]}^k := \mathbf{w}_{[(t)+l]}^k - \gamma_{[(t)]} \frac{1}{K'} \sum_{k=1}^{K'} \Delta_{[(t)+l]}^k,$$

12: **end for**

13: all-reduce aggregation of the gradients

$$\Delta_{[(t)]}^k := \mathbf{w}_{[(t)]}^k - \mathbf{w}_{[(t)+H^b]}^k.$$

14: get new global (synchronized) model $\mathbf{w}_{[(t+1)]}^k$ for all K nodes:

$$\mathbf{w}_{[(t+1)]}^k := \mathbf{w}_{[(t)]}^k - \gamma_{[(t)]} \frac{1}{K} \sum_{i=1}^K \Delta_{[(t)]}^k.$$

15: **end for**

16: **end for**

D.3. Hierarchical Local SGD Training

Now we move to our proposed training scheme for distributed heterogeneous systems. In our experimental setup, we try to mimic the real world setting where several compute devices such as GPUs are grouped over different servers, and where network bandwidth (e.g. Ethernet) limits the communication of updates of large models. The investigation of hierarchical local SGD again trains ResNet-20 on CIFAR-10 and follows the same training procedure as local SGD where we re-formulate below.

The experiments follow the common mini-batch SGD training scheme for CIFAR (He et al., 2016a;b) and all competing methods access the same total amount of data samples regardless of the number of local steps or block steps. More precisely, the training procedure is terminated when the distributed algorithms have accessed the same number of samples as a standalone worker would access in 300 epochs. The data is partitioned among the GPUs and reshuffled globally every epoch. The local mini-batches are then sampled among the local data available on each GPU. The learning rate scheme is the same as in (He et al., 2016a), where the initial learning rate starts from 0.1 and is divided by 10 when the model has accessed 50% and 75% of the total number of training samples. In addition to this, the momentum parameter is set to 0.9 without dampening and applied independently to each local model.

D.3.1. THE PERFORMANCE OF HIERARCHICAL LOCAL SGD.

Table 7. Training CIFAR-10 with ResNet-20 via local SGD on a 8×2 -GPU cluster. The local batch size B_{loc} is fixed to 128 with $H^b = 1$, and we scale the number of local steps H from 1 to 1024. The reported **training times** are the average of three runs and all the experiments are under the same training configurations for the equivalent of 300 epochs, without specific tuning.

$H =$	1	2	4	8	16	32	64	128	256	512	1024
Training Time (minutes)	20.07	13.95	10.48	9.20	8.57	8.32	9.22	9.23	9.50	10.30	10.65

Training time vs. local number of steps. Table 7 shows the performance of local SGD in terms of training time. The communication traffic comes from the global synchronization over 8 nodes, each having 2 GPUs. We can witness that increasing the number of local steps over the “datacenter” scenario cannot infinitely improve the communication performance, or would even reduce the communication benefits brought by a large number of local steps. *Hierarchical local SGD with inner node synchronization reduces the difficulty of synchronizing over the complex heterogeneous environment, and hence enhances the overall system performance of the synchronization. The benefits are further pronounced when scaling up the cluster size.*

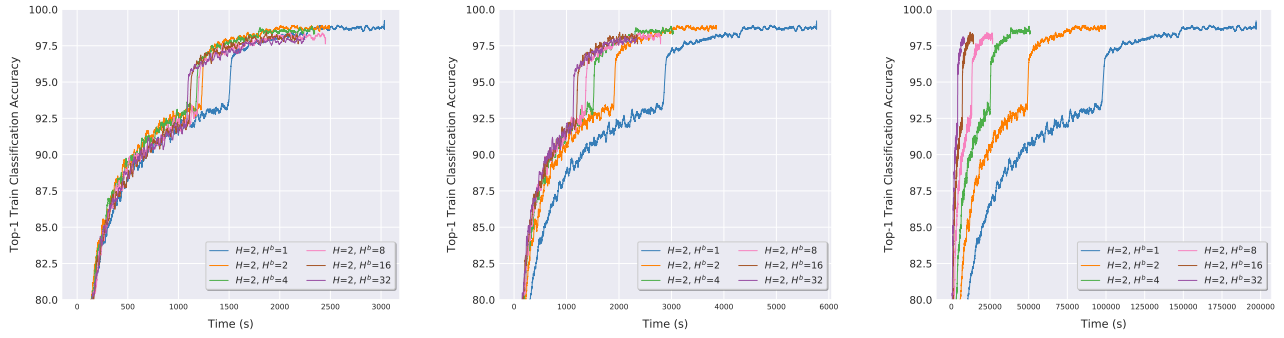


Figure 20. The performance of **hierarchical local SGD** trained on CIFAR-10 with ResNet-20 (2×2 -GPU). Each GPU block of the hierarchical local SGD has 2 GPUs, and we have 2 blocks in total. Each figure fixes the number of local steps but varies the number of block steps from 1 to 32. All the experiments are under the same training configurations without specific tuning.

Hierarchical local SGD shows high tolerance to network delays. Even in our small-scale experiment of two servers and each with two GPUs, *hierarchical local SGD shows its ability to significantly reduce the communication cost by*

increasing the number of block step H^b (for a fixed H), with trivial performance degradation. Moreover, hierarchical local SGD with a sufficient number of block steps offers strong robustness to network delays. For example, for fixed $H = 2$, by increasing the number of H^b , i.e. reducing the number of global synchronizations over all models, we obtain a significant gain in training time as in Figure 20(a). The impact of a network of slower communication is further studied in Figure 20(b), where the training is simulated in a realistic scenario and each global communication round comes with an additional delay of 1 second. Surprisingly, even for the global synchronization with straggling workers and has occurred a much more severe 50 seconds delay per global communication round, Figure 20(c) demonstrates that a large number of block steps (e.g. $H^b = 16$) still manages to fully overcome the communication bottleneck with no/trivial performance damage.

Table 8. The performance of training **CIFAR-10** with **ResNet-20** via **hierarchical local SGD** on a 16-GPU Kubernetes cluster. We simulate three different types of cluster topology, namely 8 nodes with 2 GPUs/node, 4 nodes with 4 GPUs/node, and 2 nodes with 8 GPUs/node. The configuration of hierarchical local SGD satisfies $H \cdot H^b = 16$. All variants either synchronize within each node or over all GPUs, and the communication cost is estimated by only considering $H \cdot H^b = 16$ model updates during the training (the update could come from a different level of the synchronizations). The reported results are the average of three runs and all the experiments are under the same training configurations, training for the equivalent of 300 epochs, without specific tuning.

	$H = 1, H^b = 16$	$H = 2, H^b = 8$	$H = 4, H^b = 4$	$H = 8, H^b = 2$	$H = 16, H^b = 1$
# of sync. over nodes	1	1	1	1	1
# of sync. within node	15	7	3	1	0
Test acc. on 8×2 -GPU	90.02 ± 0.28	90.25 ± 0.08	89.95 ± 0.19	91.41 ± 0.23	
Test acc. on 4×4 -GPU	91.65 ± 0.06	91.26 ± 0.17	91.46 ± 0.24	91.91 ± 0.16	91.18 ± 0.02
Test acc. on 2×8 -GPU	92.14 ± 0.10	92.05 ± 0.14	91.94 ± 0.09	91.56 ± 0.18	

Hierarchical local SGD offers improved scaling and better test accuracy. Table 8 compares the mini-batch SGD with hierarchical local SGD for fixed product $H \cdot H^b = 16$ under different network topologies, with the same training procedure. We can observe that for a heterogeneous system with a sufficient block size, hierarchical local SGD with a sufficient number of block update steps can further improve the generalization performance of local SGD training. More precisely, when $H \cdot H^b$ is fixed, hierarchical local SGD with more frequent inner-node synchronizations ($H^b > 1$) outperforms local SGD ($H^b = 1$), while still maintaining the benefits of significantly reduced communication by the inner synchronizations within each node. In summary, as witnessed by Table 8, *hierarchical local SGD outperforms both local SGD and mini-batch SGD in terms of training speed as well as model performance*, especially for the training across nodes where inter-node connection is slow but intra-node communication is more efficient.

E. Communication Schemes

This section evaluates the communication cost in terms of the number of local steps and block steps, and formalizes the whole communication problem below.

Assume K computing devices uniformly distributed over K' servers, where each server has $\frac{K}{K'}$ devices. The hierarchical local SGD training procedure will access N total samples with local mini-batch size B , with H local steps and H^b block steps.

The MPI communication scheme (Gropp et al., 1999) is introduced for communication cost evaluation. More precisely, we use general all-reduce, e.g., *recursive halving and doubling algorithm* (Thakur et al., 2005; Rabenseifner, 2004), for gradient aggregation among K computation device. For each all-reduce communication, it introduces $C \cdot \log_2 K$ communication cost, where C is the message transmission time plus network latency.

The communication cost under our hierarchical local SGD setting is mainly determined by the number of local steps and block steps. The $\frac{K}{T}$ models within each server synchronize the gradients for every H local mini-batch, and it only performs global gradients aggregation of K local models after H^b block updates. Thus, the total number of synchronizations among compute devices is reduced to $\lceil \frac{N}{KB \cdot HH^b} \rceil$, and we can formulate the overall communication cost \tilde{C} as:

$$\tilde{C} \approx \left(\lceil \frac{N}{KB \cdot H} \rceil - \lceil \frac{N}{KB \cdot HH^b} \rceil \right) \cdot C_1 \cdot K' \log_2 \frac{K}{K'} + \lceil \frac{N}{KB \cdot HH^b} \rceil \cdot C_2 \log_2 K \quad (8)$$

where C_1 is the single message passing cost for compute devices within the same server, C_2 is the cost of that across

servers, and obviously $C_1 \ll C_2$. We can easily witness that the number of block step H^b is more deterministic in terms of communication reduction than local step H . Empirical evaluations can be found in Section D.3.

Also, note that our hierarchical local SGD is orthogonal to the implementation of gradient aggregation (Goyal et al., 2017) optimized for the hardware, but focusing on overcoming the aggregation cost of more general distributed scenarios, and can be easily integrated with any optimized all-reduce implementation.

F. Discussion and Future Work

Data distribution patterns. In our experiments, the dataset is globally shuffled once per epoch and each local worker only accesses a disjoint part of the training data. Removing shuffling altogether, and instead keeping the disjoint data parts completely local during training might be envisioned for extremely large datasets which can not be shared, or also in a federated scenario where data locality is a must for privacy reasons. This scenario is not covered by the current theoretical understanding of local SGD, but will be interesting to investigate theoretically and practically.

Better learning rate scheduler. We have shown in our experiments that local SGD delivers consistent and significant improvements over the state-of-the-art performance of mini-batch SGD. For ImageNet, we simply applied the same configuration of “large-batch learning tricks” by (Goyal et al., 2017). However, this set of tricks was specifically developed and tuned for mini-batch SGD only, not for local SGD. For example, scaling the learning rate w.r.t. the global mini-batch size ignores the frequent local updates where each local model only accesses local mini-batches for most of the time. Therefore, it is expected that specifically deriving and tuning a learning rate scheduler for local SGD would lead to even more drastic improvements over mini-batch SGD, especially on larger tasks such as ImageNet.

Adaptive local SGD. As local SGD achieves better generalization than current mini-batch SGD approaches, an interesting question is if the number of local steps H could be chosen adaptively, i.e. change during the training phase. This could potentially eliminate or at least simplify complex learning rate schedules. Furthermore, recent work by (Loshchilov & Hutter, 2016; Huang et al., 2017) leverages cyclic learning rate schedules either improving the anytime performance of deep neural network training, or ensembling multiple neural networks at no additional training cost. Adaptive local SGD could potentially achieve similar goals with reduced training cost.

Hierarchical local SGD design with cluster topology. Hierarchical local SGD provides a simple but efficient training solution for devices over the complex heterogeneous system. However, its performance might be impacted by the cluster topology. For example, the topology of 8×2 -GPU in Table 8 fails to further improve the performance of local SGD by using more frequent inner node synchronization. On the contrary, sufficient large size of the GPU block could easily benefit from the block update of hierarchical local SGD, for both of communication efficiency and training quality. The design space of hierarchical local SGD for different cluster topologies should be further investigated, e.g., to investigate the two levels of model averaging frequency (within and between blocks) in terms of convergence, and the interplay of different local minima in the case of very large number of local steps.